Engineering Structures 275 (2023) 115337

Contents lists available at ScienceDirect

Engineering Structures

journal homepage: www.elsevier.com/locate/engstruct

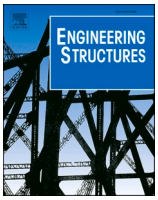

Enhanced progressive collapse resistance of bolted beam-to-column connections with ductile stainless steel components

Yuchen Song [a], Michael C.H. Yam [a,b], Junjie Wang [a,*]

[a] Department of Building and Real Estate, The Hong Kong Polytechnic University, Hong Kong SAR, China
[b] Chinese National Engineering Research Centre for Steel Construction (Hong Kong Branch), The Hong Kong Polytechnic University, Hong Kong SAR, China

ARTICLE INFO

Keywords:
Progressive collapse
Bolted beam-to-column connection
Stainless steel
Ductile fracture
Finite element analysis

ABSTRACT

With the use of ductile stainless steel bolts and hot-rolled sections/plates as critical connection components, the progressive collapse resistance of bolted beam-to-column connections may be effectively enhanced at relatively low costs. To verify the viability of this concept, a comprehensive numerical study is performed to investigate the collapse-resisting performances of flush end-plate (FEP) and web angle (WA) connections equipped with stainless steel components. Through a detailed parametric study with various connection configurations and structural layouts, it is proved that the use of stainless steel components can produce remarkable enhancement to the collapse resistance of the connections. The average increase in dynamic load capacity is 30% for FEP connections using stainless steel bolts instead of carbon steel bolts. This average ratio can be as large as 109% for WA connections with the use of stainless steel bolts and web angles. These results clearly demonstrate the great potential of using stainless steel components in steel connections for collapse-resisting purposes. Similar concepts may be naturally applied in many other scenarios where the ductility of a few critical components controls the robustness of the entire system.

1. Introduction

Progressive collapse is a phenomenon in which local structural damage spreads successively to adjacent structural components, eventually leading to a collapse that is disproportionate to the initial damage [1]. For steel and composite frames under local column removal scenarios, the spread of initial damages could be prevented by providing alternative load paths to redistribute the load previously resisted by the failed columns [1,2]. Such paths are generally realised through three load-carrying mechanisms: 1) flexural mechanism [3]; 2) tensile catenary action of floor beams [2]; and 3) tensile membrane action of floor slabs [2,4]. Experimental evidences have shown that the progressive collapse resistance of steel and composite frames mainly depends on the development of catenary and membrane actions, which are frequently limited by the ductility of the beam-to-column connections located in the bays directly affected by the removed columns [5–14]. To this concern, a great deal of research [15–20] has been devoted to investigating the ultimate behaviour and ductility of different beam-to-column connections under combined flexure and tension. In addition, strengthening strategies for beam-to-column connections have been proposed to enhance their resistance/robustness against progressive collapse. Typical examples involve optimisations of connection configuration [21–23], or providing additional load paths through installing extra structural components, such as cover plate or shear plates with slotted bolt holes [23–25], steel strands [25,26], steel rods [27], corrugated steel plates [28], and kinked bars [29] etc. However, the adoption of such strategies is usually impeded by excessive cost or significant alternations to established design principles.

Owing to its excellent corrosion resistance and aesthetic appearance, stainless steel has long been applied in seaside, offshore and bridge structures, as well as facades and skins of building structures [30]. In addition, some stainless steel categories, especially austenitic stainless steels, are known to possess high ductility and strong strain-hardening [31,32]. These characteristics may benefit the structural performance under seismic and progressive collapse scenarios, where a few critical connections or members are subjected to large ductility demands. In this light, Di Sarno et al. [33–35] investigated the improved seismic performance of steel frames with stainless steel members. Culache et al. [36] and Satheeskumar and Davison [37] examined the potential of using stainless steel bolts for enhancing the structural robustness in impact and fire scenarios. Tests conducted by the first author [38,39] recorded the maximum elongations of stainless steel bolts being up to 9

* Corresponding author.
E-mail address: junjie.wang@polyu.edu.hk (J. Wang).

https://doi.org/10.1016/j.engstruct.2022.115337
Received 25 August 2022; Received in revised form 27 October 2022; Accepted 18 November 2022
Available online 28 November 2022

times greater than that of a Grade 8.8 carbon steel bolt, which could be useful for progressive collapse prevention. More recently, experimental tests have shown the high rotation capacities of stainless steel [40–45] and composite stainless steel–concrete [46] beam-to-column joints. However, since these joint tests were all performed under pure flexural action, direct conclusions were not drawn regarding the connection performance under progressive collapse scenarios, where the catenary (tensile) action could be dominant. In this regard, a pilot analysis was performed by Wang et al. [47] on stainless steel–concrete composite frames under different column removal scenarios. A modified dynamic increase factor was proposed for the robustness assessment of such structures. Vasdravellis and his co-workers recently proposed and verified [48,49] the use of hourglass-shaped stainless steel pins for retrofitting steel joints against progressive collapse. Excellent performances were observed in the experimental tests, mainly owing to the high ductility of stainless steel devices. However, this method is again challenged by the high manufacturing cost and significant changes to the original connection configuration. Accounting for the balance of performance and cost-efficiency, a more promising strategy may be the direct replacement of critical connection components (expected to undergo large deformations) with corresponding stainless steel ones. This method would be suitable for both new constructions and retrofitting of existing structures, with minimum disturbance to established design and construction practices. The expected cost of this method is significantly lower than the others: since the replacements are limited to a small amount of critical components using commercially available stainless steel products.

Based on the above discussions, it is clear that the research on using stainless steel for progressive collapse-resisting purposes is still rather scarce in comparison with its great potential. Specifically, the performance of common beam-to-column connections with stainless steel components, against typical progressive collapse scenarios (e.g. column removal), has not been quantitatively evaluated before. In this light, this paper presents a pilot numerical study on the progressive collapse resistance of bolted beam-to-column connections, equipped with ductile stainless steel components. Two common types of bolted connection, namely flush end-plate (FEP) and web angle (WA) connections were considered in this study, representing typical semi-continuous and normally pinned configurations. Based on the viability and effectiveness concerns, the application of stainless steel is confined in bolts and bolted web angles in this study. The use of stainless steel end-plates in FEP connections is not considered, which is primarily due to the extra processes and costs required for welding stainless steel end-plates to carbon steel beams [50], hence making it less favourable for engineering practice. Finally, it should be noted that some special considerations are needed for the use of stainless steel components in steel structures. First and foremost, joining stainless steel components to carbon steel members may raise the issue of galvanic corrosion (also known as bimetallic corrosion), which could accelerate the corrosion in the less noble metal (carbon steel), hence detriment the overall durability of the structure. In the proposed connections, the galvanic corrosion issue could be handled by proper insulating the stainless steel and carbon steel components, or coating the connected region [51]. The latter approach might be more preferable since it is very similar to conventional corrosion protection methods for carbon steel structures. Moreover, the bolt preload [52] and slip factor [45,53,54] could be different in stainless steel bolted connections compared with those in carbon steel connections. However, these will be not discussed further since only snug-tight connections are considered in this study.

The results reported in this paper provide the much-needed information of to what extent can the use of stainless steel components enhance the overall progressive collapse resistance of connections. The findings may open a new horizon for developing innovative and cost-efficient collapse resisting strategies using various types of stainless steel components.

2. Ductility and material models of stainless steel and carbon steel components

This section first introduces the superior ductility of austenitic stainless steel components, which is of critical importance to the proposed concept. It should be noted that other common categories of stainless steel, including ferritic and duplex grades, are less suitable for collapse-resisting applications since their ductility is only slightly higher than that of carbon steels. Therefore, in the remaining of this paper, the term “stainless steel” will be denoting austenitic stainless steel unless stated otherwise.

Fig. 1(a) and (b) show the test results (axial tension) of typical stainless steel and carbon steel materials in hot-rolled (plates or sections) [44,55] and bolt [38] conditions. It can be clearly identified that the stainless steel materials exhibit remarkably higher deformation capacity than their carbon steel counterparts. Specifically, an A4-80 stainless steel (partially threaded) bolt reaches a maximum elongation as large as 7 times greater than that of a Grade 8.8 (G 8.8) carbon steel bolt (Fig. 1(b)). Such high ductility of stainless steel bolts is attributed to its unique failure mode, with fracture occurs in the unthreaded shank after considerable elongation and necking [38] (see Fig. 1(b)). In comparison, a carbon steel (G 8.8) bolt always fractures in the threaded portion, which is more brittle and generally has shorter deformable length as well. The specific failure mode of stainless steel bolts was consistently observed in the tests of A4-70 and A4-80 (austenitic) bolts [36,38,56], which is owing to the strong work hardening characteristic of austenitic stainless steel, leading to higher load capacity of the threaded portion (that is subjected to cold rolling during manufacturing) as compared with the unthreaded shank [38]. It should be noted that this specific failure mode was not always observed for duplex stainless steel bolts [39,56], due to the less significant work-hardening of duplex stainless steel compared with the austenitic counterparts.

Proper constitutive and fracture models for stainless steel and carbon steel components are pivotal to accurately simulating their ultimate behaviours under progressive collapse scenarios. In this study, a true stress–strain model capable of capturing the full-range material response up to fracture [38,39,44] was adopted. The model can be expressed as:

$$\begin{cases} \varepsilon_t = ln(1+\varepsilon), \sigma_t = \sigma(1+\varepsilon) (\varepsilon \le \varepsilon_u) \\ \sigma_t = \sigma_{t,u}\left[we^{\left(\varepsilon_t - \varepsilon_{t,u}\right)} + (1-w)\right] (\varepsilon > \varepsilon_u) \end{cases} \tag{1}$$

where ε and σ are the engineering strain and stress, while the subscript t denotes the corresponding true values; ε_u ($\varepsilon_{t,u}$) and σ_u ($\sigma_{t,u}$) are the engineering (true) strain/stress at necking. The first expression of Eq. (1) is the well-known relationship between engineering and true stress-strains before the onset of necking. The second expression, on the other hand, gives the post-necking true stress–strain relationship, where w is a factor controlling the shape of the stress–strain curve:

$$w = 1/\left[1 + a_1\left(\varepsilon_t - \varepsilon_{t,u}\right)^{a_2}\right] \tag{2}$$

It should be noted that the true stress–strain relationship after necking cannot be explicitly determined from the engineering stress–-strain due to the strain localisation and triaxial stress state in the necking zone. For this reason, the factor w (with two controlling parameters a_1 and a_2) was derived through a trial-and-error process: different values of a_1 and a_2 were trialled until a satisfactory matching is achieved between the tested post-necking behaviour and the parallel FE simulation, as shown in Fig. 1(a) and (b).

In companion with the full-range true stress–strain, the void-growth model (VGM) [58] was adopted for the fracture simulation of the critical components that are subjected to tension-dominant ductile fractures. This model predicts the initiation of fracture when the following criterion is satisfied:

$$\omega_F = \int \frac{d\varepsilon_{pl}}{\varepsilon_{pl,frac}} = 1 \tag{3}$$

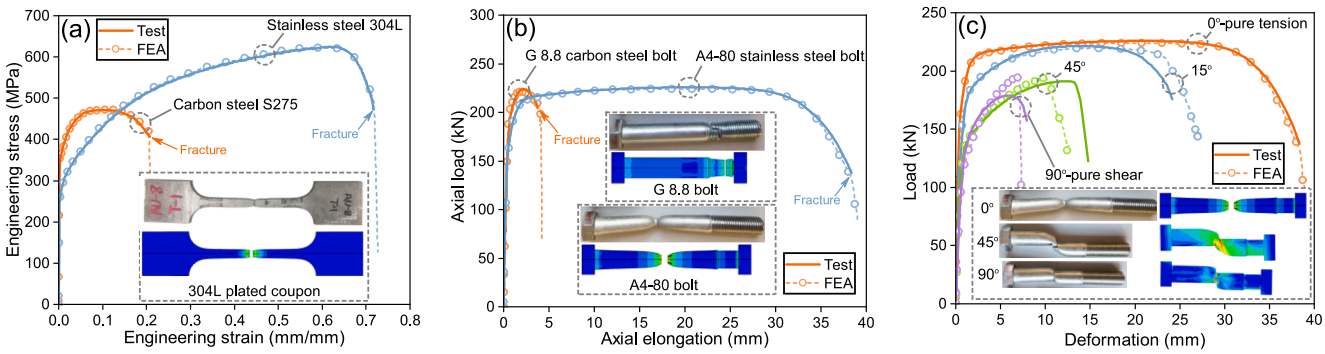

Fig. 1. Calibration of constitutive and fracture models: (a) engineering stress–strain curves of hot-rolled carbon and stainless steel plates (angles) [44,55]; (b) load-elongation curves of carbon and stainless steel bolts [57]; (c) load-deformation curves of stainless steel (A4-80) bolts under different combinations of tension and shear [57].

$$\varepsilon_{pl,frac} = C_{VGM} e^{(-1.5\eta)} \tag{4}$$

where ω_F is a dimensionless fracture index ($0 \le \omega_F \le 1$) increasing monotonically with the equivalent plastic strain ε_{pl}; $\varepsilon_{pl,frac}$ is the plastic strain at fracture corresponding with a given stress triaxiality η; The integration of Eq. (3) accounts for the variation of triaxiality (hence the variation of $\varepsilon_{pl,frac}$) throughout the loading. In Eq. (4), C_{VGM} is a material-dependent parameter needs to be calibrated by a tensile test (of standard tensile coupon or bolt) and the parallel FE simulation. As detailly outlined in Ref. [57], C_{VGM} can be determined by substituting the histories of ε_{pl} and η of the critical element (where fracture first occurs, typically located at the geometric centre of a specimen in tension), obtained from the FE simulation, into Eqs. (3) and (4). The integration in Eq. (3) should be performed up to the first fracture, which can be identified by a sudden load drop (corresponding to break of the test piece) on the test curve (Fig. 1(a) and (b)).

During the analyses of WA connections, it was noticed that the shear effect of stainless steel bolts cannot be neglected in simulating bolt fracture (this will be further discussed in Section 5.2). In such scenarios, a fracture criterion capable of predicting bolt fractures under combined tension and shear [38,59,60] was adopted instead of VGM. The expression of the criterion is similar to that of VGM, with the fracture strain (Eq. (4)) being modified to account for an additional parameter related to shear-dominant fractures under low triaxialities:

$$\varepsilon_{pl,frac} = \begin{cases} \infty, \eta \le -1/3 \\ C_1/(1+3\eta), -1/3 < \eta \le 0 \\ C_1 + (C_2 - C_1)(\eta/\eta_0)^2, 0 < \eta \le 1/3 \\ C_2\eta_0/\eta, \eta > 1/3 \end{cases} \tag{5}$$

This criterion contains two parameters C_1 and C_2, which can be calibrated by two bolt tests under pure tension and pure shear, respectively. These parameters were calibrated and validated against tests of A4-80 bolts under various angles, producing different combinations of tension and shear [57] (Fig. 1(c)). Detailed calibration process has been presented elsewhere [38,44,57] hence not repeated here.

Table 1 summarises the fracture and constitutive parameters for different stainless steel and carbon steel components calibrated based on previous material tests [44,55,57,61], which will be adopted in the remaining analyses in this study.

3. Finite element modelling

3.1. Description of FE model

To evaluate the progressive collapse-resisting performance of beam-to-column connections with and without stainless steel components, a series of quasi-static push-down analyses under middle column removal were performed. Fig. 2 illustrates the prototype structure (plane frame) for these analyses, where only a half structure is shown due to symmetry. It should be noted that the out-of-plane restraints provided by the transverse beams (and their connections) and the composite floor slabs also contribute to the progressive collapse resistance of the entire system [2,4,62,63]. However, since the objective of this work is to evaluate the performance of beam-to-column connections, the out-of-plane effects were ignored to enable the isolation of the connection behaviour. Similar treatments can be also found in previous works focusing on the progressive collapse performance of beam-to-column connections [14,15,19].

In a middle column removal scenario, the nearest beam spans on

Table 1
Calibrated constitutive and fracture parameters of materials.

Material	Elastic modulus (GPa)	Yield stress (MPa)	True strain at necking $\varepsilon_{t,u}$ (mm/mm)	True stress at necking $\sigma_{t,u}$ (MPa)	Post-necking parameters a_1	a_2	Fracture parameters C_{VGM}	
Hot-rolled S275 [55]	210	350	0.134	538.1	2.0	1.0	1.2	
Hot-rolled 304L [44]	190	256	0.470	993.2	4.0	2.0	2.5	
G 8.8 partially threaded bolt [57]	207	799	0.060	932.3	5.0	1.0	0.65	
G 8.8 fully threaded bolt [57]	207	680	0.060	1025.5	5.0	1.0	0.85	
G 10.9 partially threaded bolt [61]	210	1013	0.061	1105.4	150	2.0	1.0	
A4-80 partially threaded bolt (T[1]) [57]	188	862	0.060	1039.9	2.0	1.0	–	
							C_1	C_2
A4-80 partially threaded bolt (U[1]) [57]	188	522	0.180	851.8	1.3	2.5	0.66	2.94

[1] : "T" denotes the threaded portion of a PT bolt; "U" denotes the unthreaded portion.

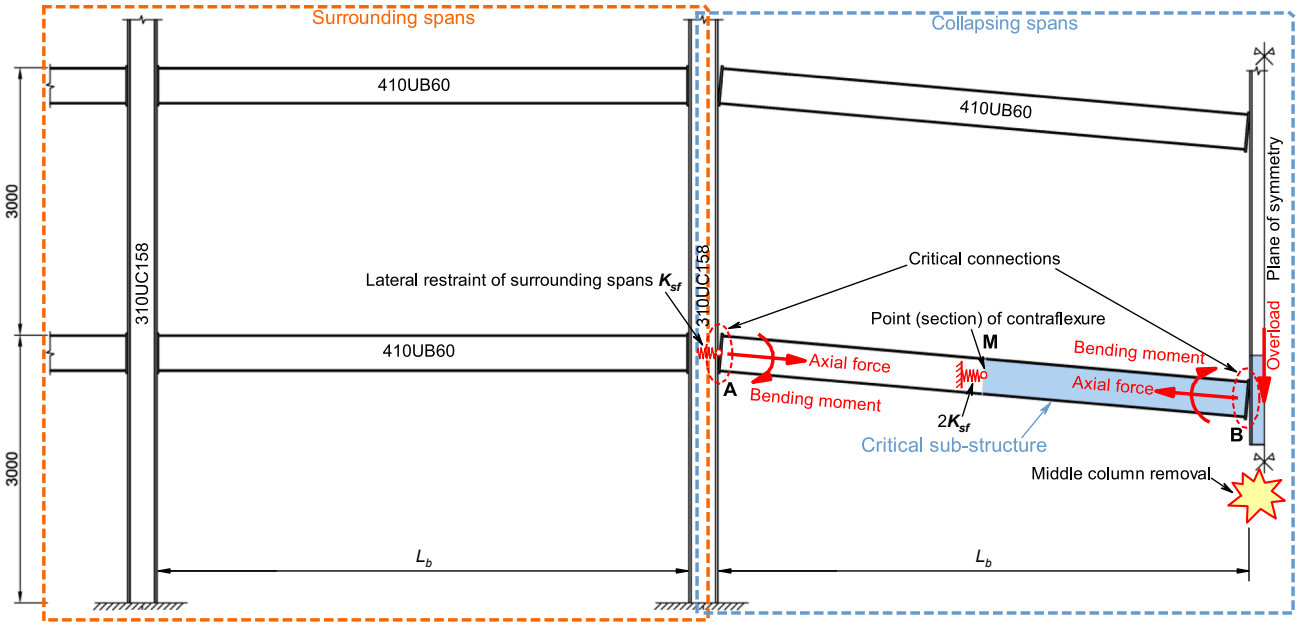

Fig. 2. Prototype structure for push-down analysis under a middle column removal scenario.

both sides of the removed column are directly affected, which are referred to as the "collapsing spans" in this study (Fig. 2). The remaining spans of the structure, namely the "surrounding spans", provide restraints to the collapsing spans. The robustness of the entire structure in this scenario largely relies on the load carrying capacity and ductility of the beam-to-column connections within the collapsing spans, namely the "critical connections". If the coupling effect between the collapsing and the surrounding spans is neglected, the lateral restraints of the surrounding spans can be idealised as a series of elastic/inelastic springs (with stiffness K_{sf}) connected to the far ends of the collapsing spans (A). Given that all the critical connections have the same configuration, and their moment-rotation behaviours are the same under positive and negative moments, each of the beams in the collapsing spans will have antisymmetric internal forces (with equal axial forces and reversed bending moments at near-end B and far-end A) [15]. Therefore, a "critical sub-structure" containing a half beam span (MB) and only one critical connection on each side of the removed column (highlighted in blue in Fig. 2) can be taken to represent the response of the collapsing spans. The end M of the critical sub-structure corresponds to the point of contraflexure at the mid-span of the beam, which can be modelled as a pin support restrained by a horizontal spring (of which the stiffness should be $2K_{sf}$ as explained below). Due to the antisymmetric internal forces within span AB, the relative deformations of the beam are also antisymmetric about the point M. Therefore, the relative horizontal movements (with respective to M) at A and B should be of equal value and opposite directions. Given the absolute horizontal movement at the near-end B is equal to zero (as there is negligible horizontal movements at the surface of the middle column), the absolute horizontal movement at end A should be two times that at mid-span M. Considering the near constant horizontal forces along span AB, the horizontal restraining stiffness (horizontal force/horizontal movement) for the critical sub-structure at M ($2K_{sf}$) should be two times that at A (K_{sf}). The validity of the above simplifications for the critical sub-structure was proved through a comparative FE analysis with full and half spans of the beam. As shown in Fig. 3, the half span model with a horizontal restraining stiffness of $2K_{sf}$ predicts a nearly identical load–displacement response to the full span model with restraining stiffness K_{sf}.

Fig. 4 shows the FE model of a critical sub-structure developed on the platform of ABAQUS [64]. Accounting for the symmetries about the YZ (mid-thickness plane of the beam and column webs) and XY (mid-depth plane of the column) planes, only a quarter of the sub-structure was modelled. The symmetric boundary condition required the surfaces (of the beam, column and end-plate) lain on the YZ plane to be restrained against movements in the X direction. On the other hand, the surfaces (of the column and its stiffeners) on the XY plane were restrained against movements in the Z direction, hence the column was only allowed to

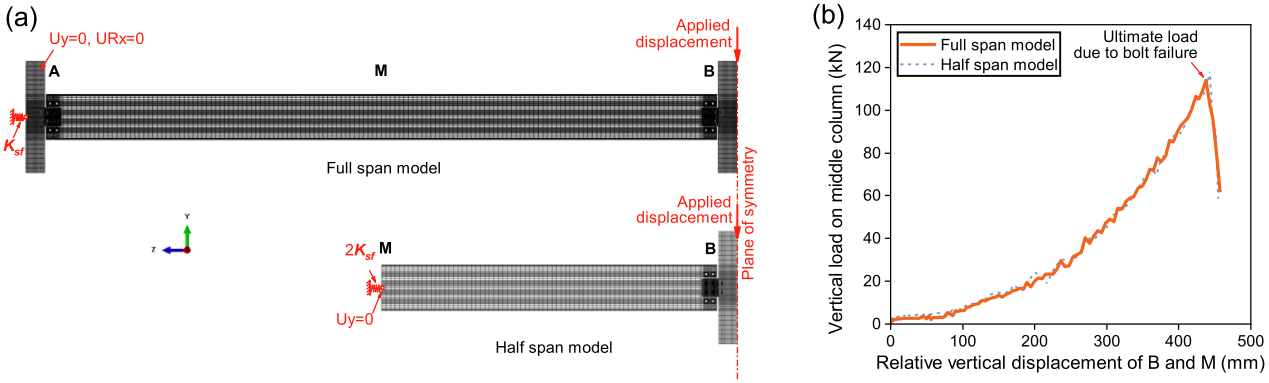

Fig. 3. Validation of the critical sub-structure: (a) FE models with full and half beam spans; (b) analysis results (vertical load-displacements).

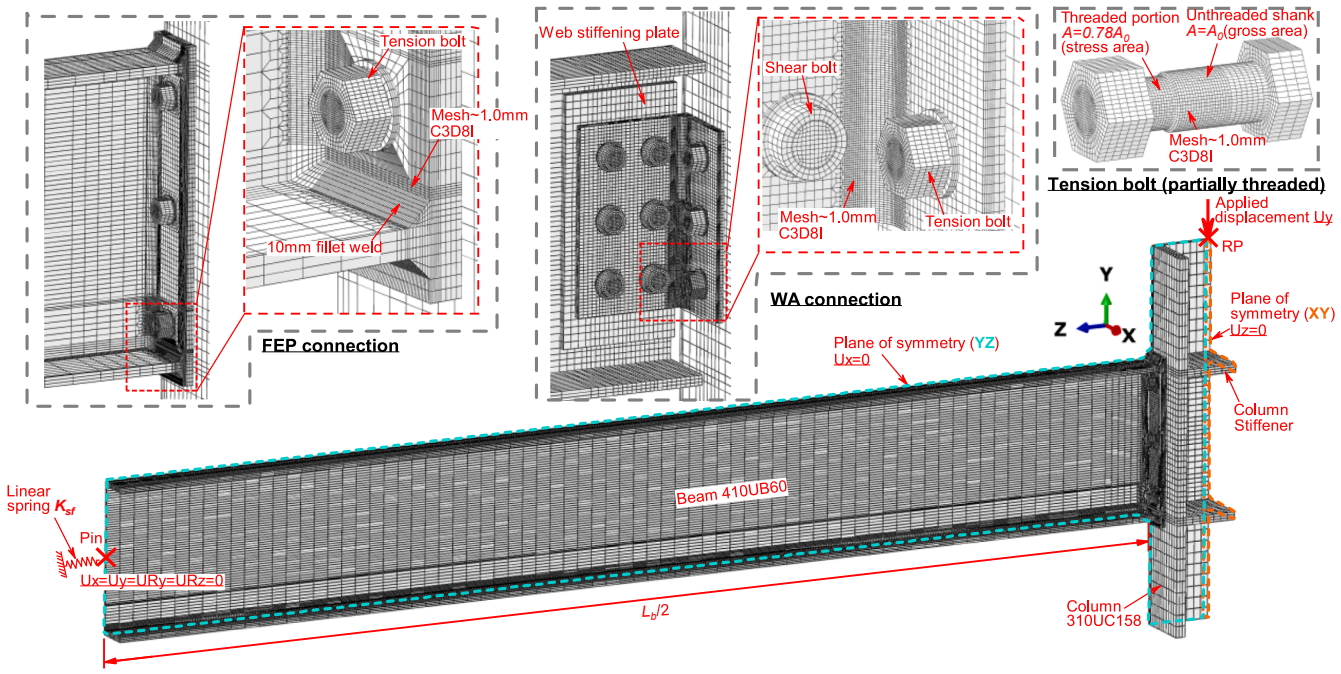

Fig. 4. FE model of a critical sub-structure.

slide in the vertical (Y) direction. The simply supported condition at the boundary of a beam (point of contraflexure) was realised through a reference point (pin) coupled with the beam cross-section, which is restrained against all degrees of freedom except the horizontal displacement (Uz) and the in-plane rotation (URx). The pin is connected to a linear spring, representing the lateral restraint acting at the point of contraflexure. The stiffness of the spring (K_{sf}) is half of that in Figs. 2 and 3 ($2K_{sf}$), since only a half of the beam cross-section is modelled (due to the symmetry about the YZ plane). The value of K_{sf} was determined based on a set of linear elastic plane frame analyses, considering different restraining conditions of the surrounding span, as shown in Fig. 5. The external load was applied via imposing vertical displacements (Uy) to a reference point (RP) coupled with the top surface of the column. A relatively short column length (1000 mm) was adopted in all the models, since the stresses and deformations were found to be negligible out of the panel zone (above and below the column web stiffeners). A work conducted by Li et al. [5] concluded that the column length has no effect on the structural behaviour of steel beam-to-column connections under a column removal scenario, where the structural behaviour can be well simulated by only allowing vertical slides of the columns.

As shown in Fig. 4, the FE models for FEP and WA connections were only differentiated in the connection region. The beam and column in each of the WA connections were separated by a gap of 15 mm. The detailed configurations of these connections are shown in Fig. 6. The constitutive parameters (true stress–strain) calibrated in Section 2 (Table 1) were input into the FE models, along with von Mises yield criterion and isotropic hardening. The simulation of fracture was enabled using the built-in "ductile damage" module (adopting the fracture criteria and parameters in Section 2) and "element deletion" option. The weld metals in the FEP models were assumed to be free from fracture, since the fillet welds were designed to be overstrength to avoid premature brittle failures prior to end-plate fractures. In line with a mesh sensitivity analysis conducted elsewhere [57], C3D8I (an 8-node 3D brick element with 8 integration points and incompatible modes) elements with 1 mm mesh size were adopted for the critical connection components where fractures are expected to take place. These include the regions close to the weld toes of end-plates and the roots of web angles, as well as all the tension bolts (connecting to the column flange). The element type and mesh size of the critical components were identical to those adopted in calibrating the material parameters (Section 2),

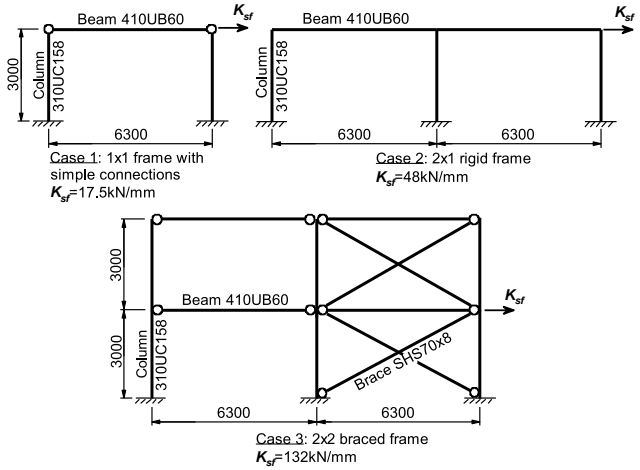

Fig. 5. Lateral restraining stiffness K_{sf} with different surrounding span conditions.

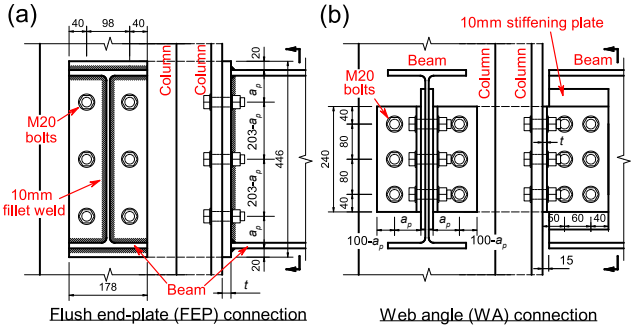

Fig. 6. Configurations of connections for parametric analysis: (a) FEP connection; (b) WA connection.

hence could minimise the potential effect of FE mesh on fracture prediction. To reduce the overall computational cost, C3D8R (with reduced integration) elements with coarser mesh sizes were applied for the other less critical components. The interactions between different components were modelled by the "general contact" option in ABAQUS. The contact behaviour in the normal direction was set to be "hard", i.e. the penetration at the contact interface is minimised; whilst the tangential contact behaviour was defined by a penalty friction formulation, with a friction coefficient of 0.2. Within the scope of this study, all the bolts in the FEP and WA connections are considered to be snug-tight, hence bolt preload was not modelled in the FEA.

With the incorporation of fracture simulation in the FEA, an implicit algorithm (ABAQUS/Standard) will encounter convergence issues, hence the post-fracture behaviour (after element deletion) will be unavailable from the analysis. To overcome this difficulty, an explicit dynamic solver (ABAQUS/Explicit) was adopted in this study, which has been commonly used for progressive collapse simulations [14,16,19,65]. In order to guarantee the quasi-static loading condition using the dynamic explicit solver, the time span was carefully selected to reduce the dynamic effect. Furthermore, mass-scaling was applied to the model to reduce the computational cost. The mass density of the smallest elements (in the critical components) was amplified artificially, increasing the size of the stable time increment (time Inc.) from approximately 5E-8 to 1E-6 s. This could in turn reduce the running time to around 1/20 of that without mass scaling. Fig. 7(a) compares the analysis results of a FEP connection with and without mass scaling, where one can see that the adoption of mass scaling has barely any effect on the load–displacement responses before and after fracture. In addition, Fig. 7(b) compares the load–displacement responses obtained through ABAQUS/Explicit (with the stable time increment scaled to 1E-6 s) and ABAQUS/Standard (static analysis) of the same FEP connection, as well as a WA connection. It can be seen that the analysis results agree very well until the terminations of the implicit algorithm (due to convergence issue). This comparison further proves the feasibility of the adopted explicit algorithm for quasi-static analyses. It should be noted that the use of explicit algorithm (either with or without mass scaling) inevitably caused some oscillations of load after a fracture (Fig. 7), which is due to the extra kinetic energy caused by the sudden drop of load. Such oscillations were gradually stabilised with the continuing of analysis before the next fracture. To facilitate the interpretation of the connection behaviour, the oscillating curves were post-processed by a Gaussian filtering algorithm. The "smoothed" curves (see Fig. 7(b)) obtained in this way are used in the remaining discussions in this study.

3.2. Model validation

The developed FE models were validated against previous experimental tests of beam-to-column connections under middle column loss scenarios. These tests contain similar connection configurations and loading conditions to the critical sub-structure modelled in this study (Fig. 4). All the test specimens are fully made of carbon steel (S275), given the lack of relevant tests of connections with stainless steel components. For FEP connections, two tests (*P*-1 and P-2) reported by Kukla and Kozlowski [19] were employed, which contain FEP connections with 10 mm or 20 mm end-plates and two rows of M20 G 10.9 bolt. On the other hand, two WA specimens tested by Yang and Tan [20] (W-8 and W-12), having 8 mm or 12 mm web angle cleats and three bolt-rows (M20 G 8.8 fully threaded bolts), were simulated to validate the WA models. Fig. 8 shows the FE models for these test specimens, where the critical dimensions and section profiles are given. Similar to the critical sub-structure shown in Fig. 4, a one-quarter model was employed for the WA specimens (Fig. 8 (b)) considering the symmetries about XY and YZ planes. The modelled boundary conditions were practically the same to those in Fig. 4, expect that the reference point (pin) was placed at a 330 mm distance to the beam end, in accordance with the actual configuration of the test rig. In modelling the FEP specimens (Fig. 8(a)), the symmetry about YZ plane was not considered, hence the model was one half of the actual geometry. This is to capture the out-of-plane deformation (buckling) of the unstiffened column web, which was observed in these tests. In both cases, the stiffness of the spring connected to the

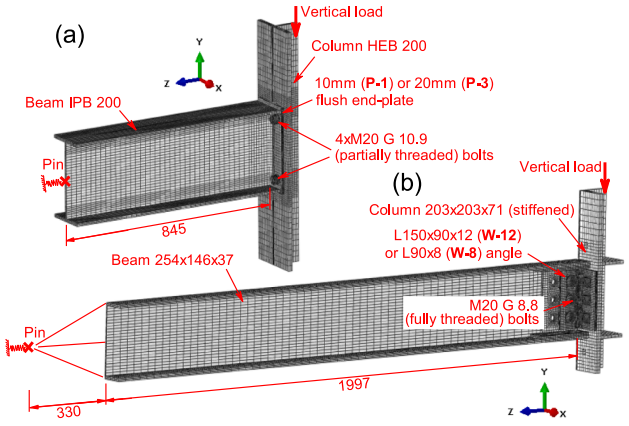

Fig. 8. FE models of previously tested specimens for validation purpose: (a) FEP connection; (b) WA connection.

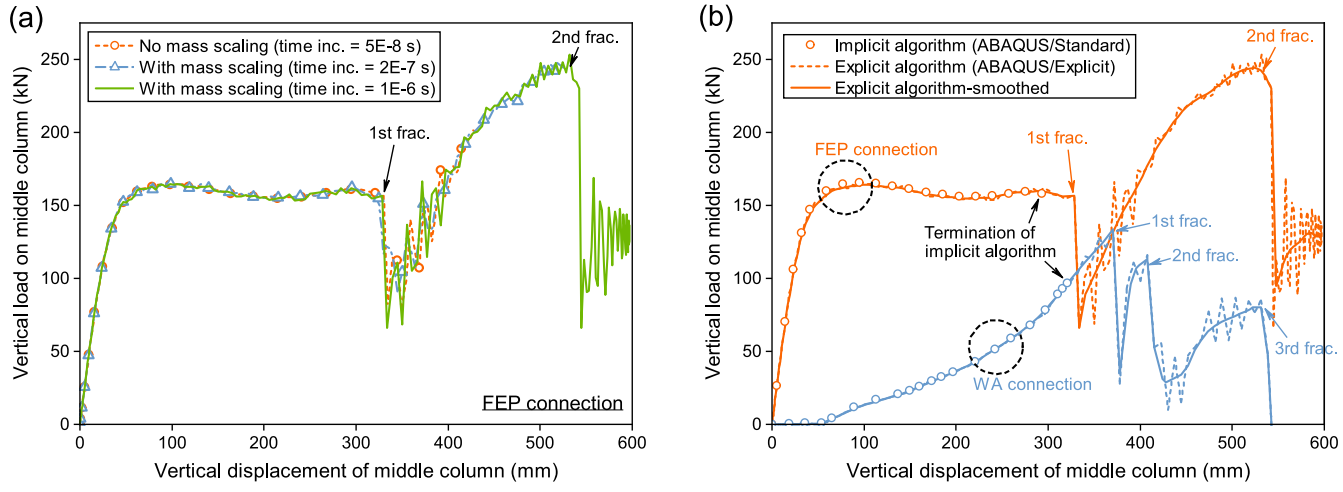

Fig. 7. Comparison of simulated load–displacement responses: (a) explicit algorithm with different mass scaling; (b) explicit and implicit algorithms.

beam end was set equal to the stiffness of the reaction system given in the test reports [19,20]. In accordance with the loading conditions in the tests, vertical displacements were applied to the tops of the columns, which is same to the load application shown in Fig. 4. Since the bolts were all snug-tightened in the tests, bolt preload was again not incorporated in the validation models. The settings of element type, mesh size and contact property are exactly the same to those described previously in Sections 3.1, hence are not repeated herein. For modelling the materials in these test specimens (S275 steel plates/sections and G 8.8/10.9 bolts), the constitutive and fracture models introduced in Section 2 were employed. The material parameters (Table 1) were calibrated by the reported stress–strain curves of the actual test materials if they are available [55]. For the G 8.8/10.9 bolts of which the stress–strain (load-deformation) curves were not reported, the bolt test results (of the same grade and diameter) reported elsewhere [57,61] were employed for calibrating the required parameters.

Fig. 9(a) compares the simulated vertical load–displacement (of the middle column) responses with the test results of the four specimens. Moreover, Fig. 9(b)-(d) present the tested and simulated failure modes. It can be seen that the overall responses of the specimens are reasonably predicted by the FEA. Final failures of the specimens were due to fractures of the web angle (W-8) or tension bolts (W-12, *P*-1 and P-2), which were also faithfully reproduced. It should be noted that in the FEA, some high Mises stresses (up to 2769 MPa, shown in the legend in Fig. 9) were reached in a small number of elements close to the fracture surfaces. These stresses are solely due to excessive distortions of the elements after fracture (element deletion), which are not related to any physical implications.

4. Parametric study of flush end-plate (FEP) connections

4.1. Overview of parameters

To evaluate the performances of FEP connections with carbon steel and stainless steel bolts, a comprehensive parametric study was carried out based on the FE model and the connection configuration shown in Fig. 4 and Fig. 6(a), respectively. Three variables related to the configuration were incorporated: (1) the end-plate thickness t; (2) the position of bolts; and (3) the number of bolt-rows. The bolt position was changed by varying the vertical distance a_p (see Fig. 6(a)) between the outer most bolt-row and the external surface of beam flanges. In addition, two parameters related to the structural layout were considered, i.e., the lateral restraining stiffness of surrounding span, K_{sf} (corresponding to three practical cases show in Fig. 5), and the clear span-to-depth ratio of beams in the prototype structure (Fig. 2). For the latter, the beam depth D_b was maintained constant (406 mm) for all the cases, whilst the clear span L_b of the beams was set to be 4000, 6000 and 8000 mm, hence obtaining L_b/D_b equal to approximately 10, 15 and 20. Table 2 summarises the combinations of parameters in this study. For each of the cases, conditions with carbon steel G 8.8 bolts (CSB) and stainless steel A4-80 bolts (SSB) (M20x80 partially threaded bolts) were analysed. All the other structural components (beam, column, end-plate etc.) were designed to be S275 carbon steel.

4.2. General connection behaviour and failure modes

The behaviour of a beam-to-column connection is largely affected by the axial force of the beam in a column removal scenario. For FEP connections, the beam axial force is initially compressive due to the contact between the end-plate and the column flange against beam rotation. The orientation of the compressive force is alone the line connecting the compressive centres at both ends of the beam, creating the so-called "arching action" (Fig. 10(a)). This beneficial effect enhances the vertical load resistance, which vanishes when the action line becomes horizontal. Thereafter, the effect of compressive axial force reduces the vertical load resistance. With further developments of chord rotation, the axial compressive force gradually decreases and finally turns into tensile due to the separation of end-plate and column, creating the "catenary action" (Fig. 10(b)). Fig. 10(c) quantitatively demonstrates the effects of beam axial force (blue curves) on the vertical load resistance (red curves) with the development of beam chord rotation. Comparing with the benchmark condition with pure flexural action ($K_{sf} = 0$), the compressive arching action (with $K_{sf} = 132$kN/mm) creates an increase in the vertical load resistance when the chord rotation is less than around 0.05 rad. The case with 2 bolt-rows (Case 2) exhibits higher compressive axial force hence greater arching action than that with 4-bolt rows (Case 14). However, in either case the vertical load capacity is still mainly contributed by the flexural action when the beam axial force is compressive. This stage is hence referred to as "flexure-dominant" in the remaining discussions. After a "transition state" (corresponding with a beam chord rotation in the range of 0.08–0.1 rad for the cases with $L_b/D_b = 15$.) where the axial force turns from compressive to tensile, the system enters the "catenary-dominant stage", which is featured by drastically increased axial force and vertical load with the increase of chord rotation (see Fig. 10(c)).

Figs. 11-13 illustrate three typical failure modes obtained for FEP connections. As shown in Fig. 11, the failure of a FEP connection with relatively thick end-plate is typically triggered by successive fractures of

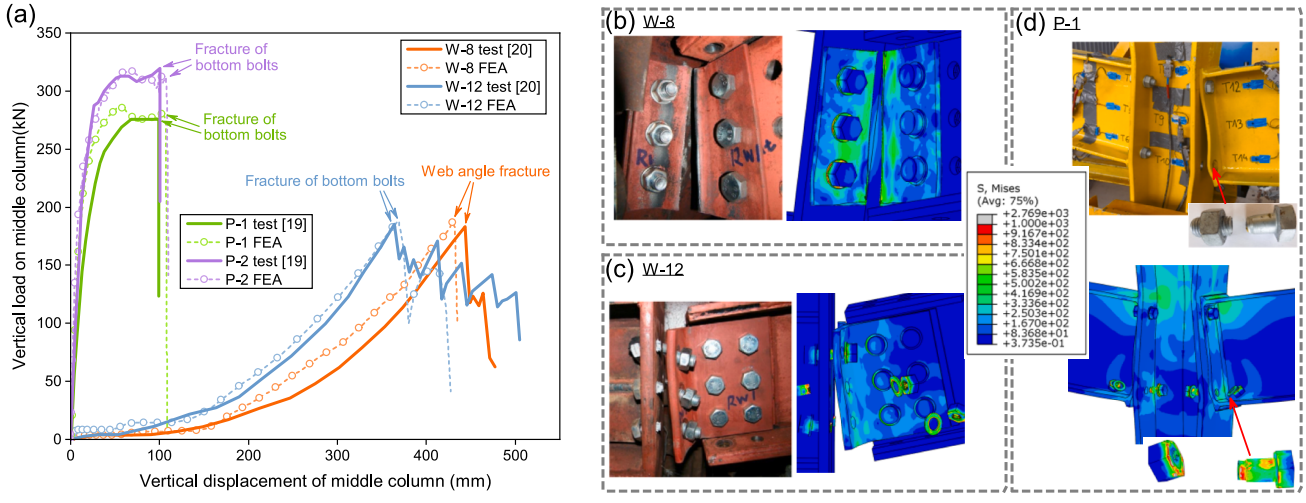

Fig. 9. Validation of FE models: (a) tested vs simulated vertical load–displacement responses; (b)-(d) comparison of failure modes obtained from tests [19,20] (permissions of reuse by ASCE and Elsevier) and FEA.

Table 2
Summary of parameters and analysed results of FEP connections.

Case No.	Configuration of connection			K_{sf} (kN/mm)	L_b/D_b	$P_{d,max}$ (kN)		$k_{P,SSB}$	Failure mode[1] (CSB/SSB)
	No. of bolt-rows	q_p (mm)	t (mm)			CSB	SSB		
1	2	73	10	132	15	94	94	1.00	FBE/FE
2	2	73	15	132	15	95	119	1.25	FB/FB
3	2	73	20	132	15	96	122	1.27	FB/FB
4	3	53	10	132	15	117	123	1.05	FBE/FE
5	3	53	15	132	15	110	162	1.47	FB/FBE
6	3	53	20	132	15	122	160	1.31	FB/FB
7	3	73	10	132	15	109	109	1.00	FBE/FE
8	3	73	15	132	15	115	165	1.44	FB/FBE
9	3	73	20	132	15	121	155	1.29	FB/FB
10	3	93	10	132	15	102	138	1.35	FBE/FE
11	3	93	15	132	15	114	171	1.50	FB/FBE
12	3	93	20	132	15	122	160	1.31	FB/FB
13	4	73	10	132	15	116	116	1.00	FBE/FE
14	4	73	15	132	15	133	225	1.69	FB/FBE
15	4	73	20	132	15	144	218	1.51	FB/FB
16	4	73	15	17.5	15	124	214	1.73	FB/FBE
17	4	73	15	48	15	127	220	1.73	FB/FB
18	4	73	15	132	10	213	284	1.33	FB/FBE
19	4	73	15	132	20	94	192	2.04	FB/FBE

[1] : Abbreviations of the failure modes: "FB"-Fracture of bolts; "FE"-Fracture of end-plate; "FBE"-Fracture of bolts with cracking in the end-plate.

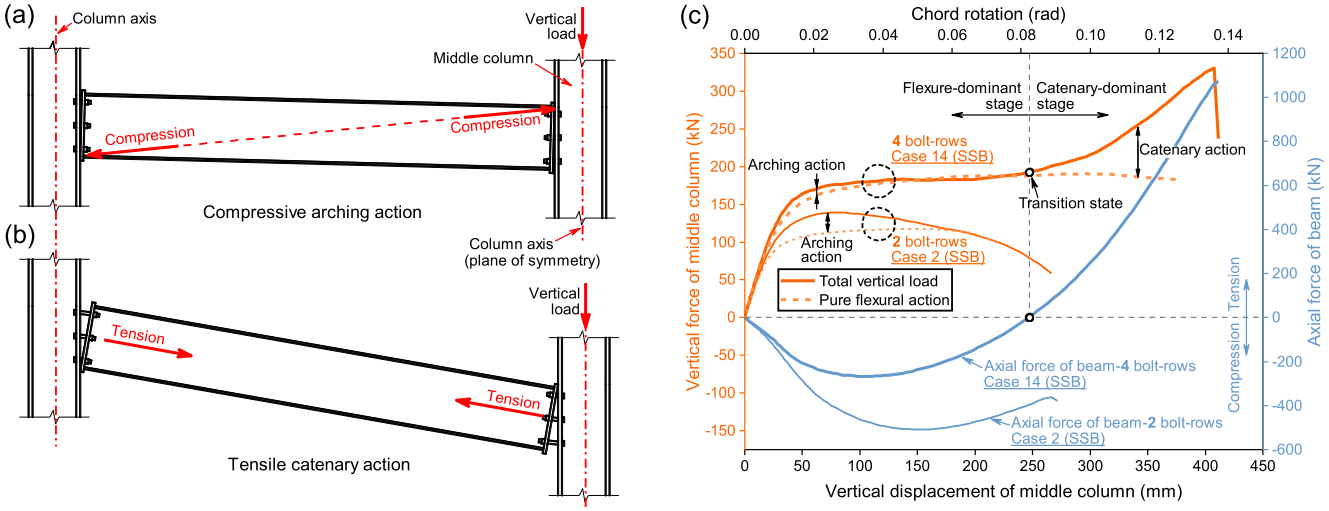

Fig. 10. Effects of axial force of beam on vertical load-carrying behaviour of FEP connections: (a) compressive arching action; (b) tensile catenary action; (c) vertical load–displacement curves with or without axial force effects.

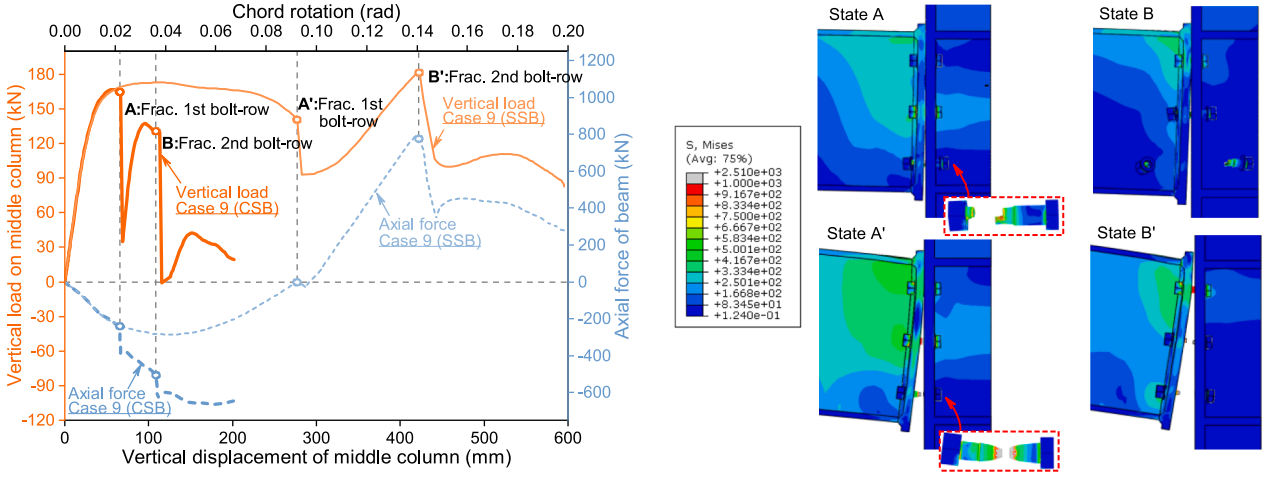

Fig. 11. Failure of FEP connections with bolt fractures (Mode FB).

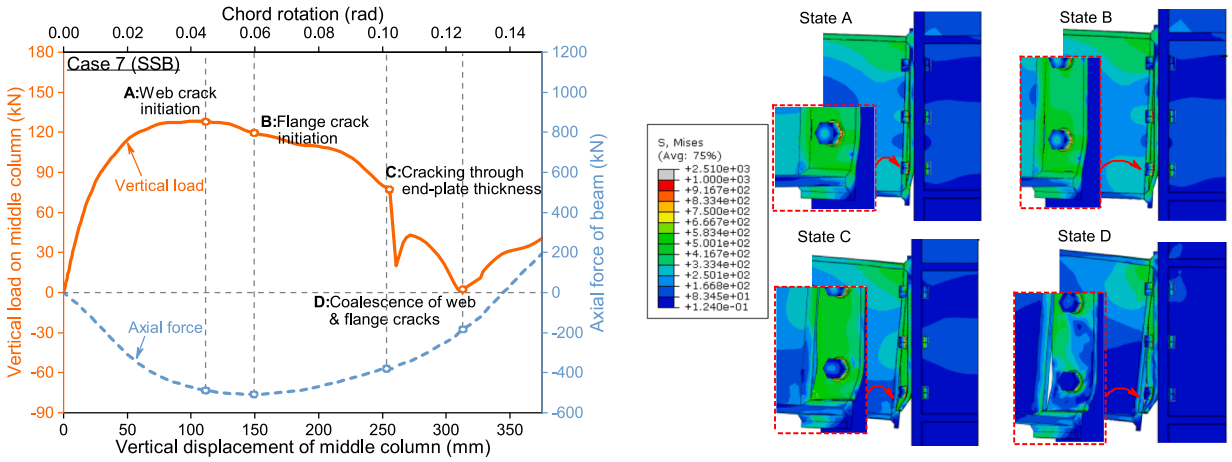

Fig. 12. Failure of FEP connections with end-plate fracture (Mode FE).

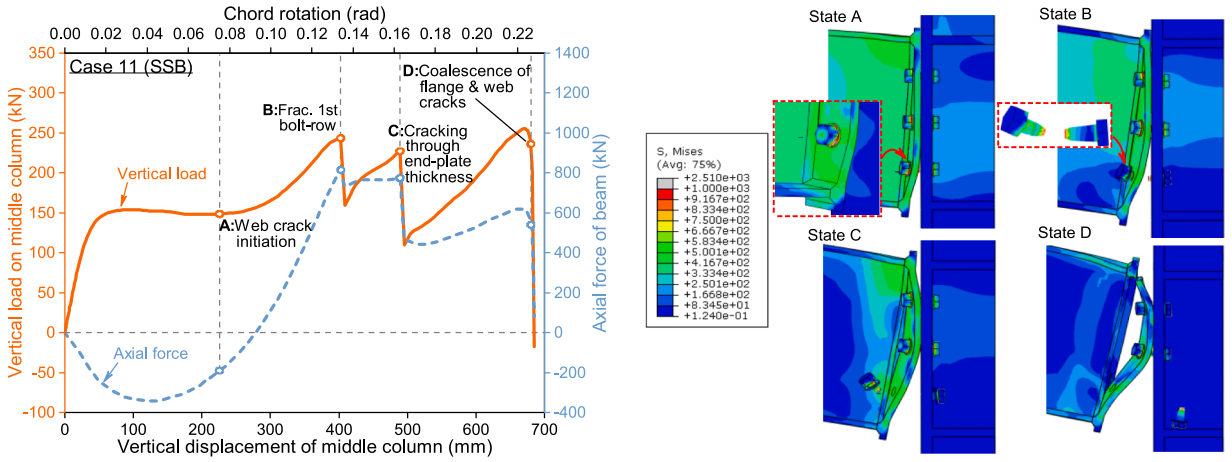

Fig. 13. Failure of FEP connections with combined fractures of bolts and end-plate (Mode FBE).

bolts from the bottom to the top (Mode FB), each corresponds with a sudden drop of vertical load. With this failure mode, distinct behaviours were observed between the connections with carbon steel bolts (CSB) and stainless steel bolts (SSB): for the former, the bolts fractured at relatively small chord rotations due to the low ductility of CSB. Since the connection was still in the flexure-dominant stage, the load-carrying capacity dropped significantly after the 1st bolt fracture (Stage A). On the other hand, a connection equipped with ductile SSB could sustain a much larger chord rotation, hence enabling the development of catenary action. Due to the catenary action, the vertical load carried by the connection with SSB increases substantially after the fracture of the 1st bolt-row (State A' in Fig. 11), leading to a higher load at the 2nd bolt fracture (State B').

For connections with relatively thin end-plates, final failure was commonly due to complete cracking of end-plates alone the fillet welds (Mode FE). This type of failure typically originates from an initial cracking adjacent t o the weld toes joining the beam web (referred to as the "web crack") or flange (flange crack), corresponding to States A and B in Fig. 12. However, short individual cracks did not lead to significant deteriorations of the load capacity, until the development of an individual crack through the end-plate thickness (State C), or the coalescence of flange and web cracks (State D). With this failure mode, the connection behaviour is less related to the ductility of the bolt, hence the use of SSB instead of CSB should have limited effects on the overall response.

In the rest of the cases, the connections failed by combined fractures of bolts and end-plates (Mode FBE). For example, the failure shown in Fig. 13 was initiated by a web crack of the end-plate (State A), followed by the fracture of the 1st bolt-row (State B), as well as the development and coalescence of end-plate cracking (States C and D). Due to the contribution of catenary action, the vertical load re-ascended immediately after States B and C. The maximum vertical load was achieved right before State D.

It should be noted that all the above discussions are based on the (quasi-) static responses of connections and sub-structures. However, in practical column removal scenarios, the structural response is actually dynamic since columns are generally removed suddenly due to blasts or external impacts. This is equivalent to a condition with suddenly applied floor loads on the affected structures directly above the removed column. To consider this effect, an energy approach proposed by Izzuddin et al. [66] was adopted to link the static and dynamic responses of sub-structures (connections). As illustrated in Fig. 14, a "pseudo-static response" can be derived by enforcing the equilibrium between the static internal energy (Area II + III in Fig. 14) and the work done by the dynamic load (Area I + II) for a series of given displacement u_d up to final failure. The peak load of the pseudo-static response, i.e. the maximum dynamic load $P_{d,\max}$, is an indicator of the maximum resistance of the sub-structure under a dynamic column removal scenario, which is taken as a primary performance index in this study. In addition, the enhancement ratio of the maximum dynamic load due to the use of SSB instead of CSB, i.e., $k_{P,SSB} = P_{d,\max,SSB}/P_{d,\max,CSB}$, can be used to evaluate the effectiveness of using stainless steel bolts for enhancing the

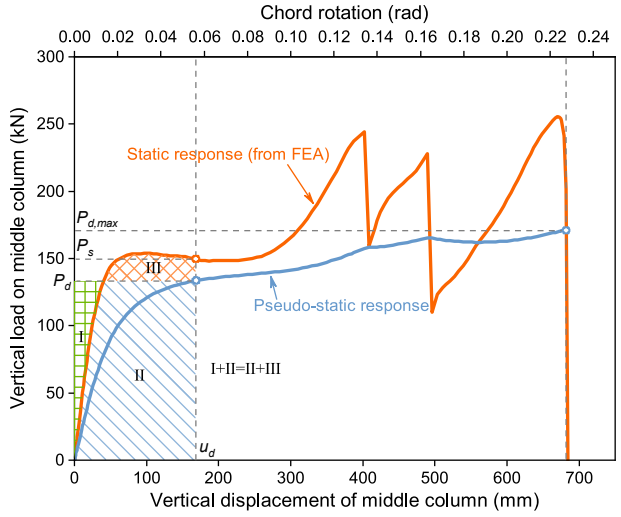

Fig. 14. Conversion of static load–displacement response to pseudo-static (dynamic) response.

collapse resistance. The calculated $P_{d,\max}$ and $k_{P,SSB}$ are summarised in Table 2 for all the analysed cases along with the identified failure modes (FB, FE or FBE).

4.3. Effect of connection configuration

Fig. 15(a) shows the static load–displacement responses of FEP connections with 10, 15 and 20 mm end-plates, where the responses of connections with carbon steel bolts (CSB) and stainless steel bolts (SSB) are compared for each of the cases. The transition states of the connections (if existed), where the behaviour turns from flexure-dominant to catenary-dominant, are marked by circles in the figure. It can be seen that the static responses with CSB and SSB only differ after the first component fracture. For the connections with 15 and 20 mm end-plates, final failure was Mode FB or FBE. In these cases, replacing the CSB with SSB postponed the final failure from the flexure-dominant to catenary-dominant stage, hence creating the "re-ascending" response after the 1st bolt fracture. Using either CSB or SSB had limited effects on the overall response when the failure mode is FE (with a 10 mm end-plate): since in either condition the failure was triggered by premature end-plate cracking in the flexure-dominant stage. Hence, the ductility of SSB, as well as the potential load enhancement due to the catenary action were not fully exploited. Fig. 15(b) shows the pseudo-static responses (obtained through the method illustrated in Fig. 14) of these three cases, where the maximum dynamic loads ($P_{d,\max}$) are marked with stars. For connections failed in the flexure-dominant stage (all the connections with CSB and the t = 10 mm connection with SSB), the maximum dynamic load was attained at a relatively small displacement close to first fracture. For the rest connections failed in the catenary-dominant stage, higher dynamic loads could be attained at 2nd or 3rd fractures. As summarised in Table 2, the 15 and 20 mm FEP connections with SSB reached 44 % and 29 % higher $P_{d,\max}$ compared with the counterparts having CSB. On the other hand, the $P_{d,\max}$ remains basically unchanged for the 10 mm FEP connections with SSB or CSB.

Fig. 16(a) shows the static load–displacement responses of 15 mm FEP connections with the distance a_p (see Fig. 6(a)) equal to 53, 73 and 93 mm. It can be seen that the static load resistance in the flexure-dominant stage increases with the decrease in a_p. However, the maximum dynamic loads (See Fig. 16(b) and Table 2) of the connections with CSB are basically equal with different a_p, which is primarily due to the earlier fractures of the bolts, despite the higher static loads achieved with reduced a_p. All the connections with SSB exhibited sufficient deformation capacity to enter the catenary-dominant stage, leading to considerable enhancements in the maximum dynamic load (40–50 %) compared with the connections with CSB. Within the catenary-dominant stage, a_p seems to have limited effects on either the static or dynamic load.

The effects of bolt-row number on the static and pseudo-static load responses are demonstrated in Fig. 17. By increasing the number of bolt-rows from 2 to 4, the static load resistance was significantly enhanced in both flexure-dominant and catenary-dominant stages. The first bolt fracture was also postponed due to the force redistribution among bolt-rows (see Fig. 17(a)). Both effects contributed to the significant increase in the maximum dynamic load with the increase of bolt-row number, which can be seen in Fig. 17(b) and Table 2 (Cases 2, 8 and 14). The ratio $k_{P,SSB}$ also enhanced remarkably (from 1.25 to 1.69), demonstrating a more effective use of stainless steel bolts with an increased number of bolt-rows. It is noteworthy that with two rows of SSB, the catenary action was not activated due to the softening response of static load–displacement and the insufficient deformation capacity.

4.4. Effect of structural layout

The effect of lateral restraining stiffness K_{sf} is demonstrated through Cases 14, 16 and 17. From Fig. 18(a), it can be seen that the lateral restraining stiffness only influences the connection response in the catenary-dominant stage: with higher K_{sf}, the ascending stiffness (the slope of the curve prior to first bolt fracture) is remarkably increased. The peak static load, however, is basically not affected, though it is attained at smaller chord rotations with higher K_{sf}. With respect to the

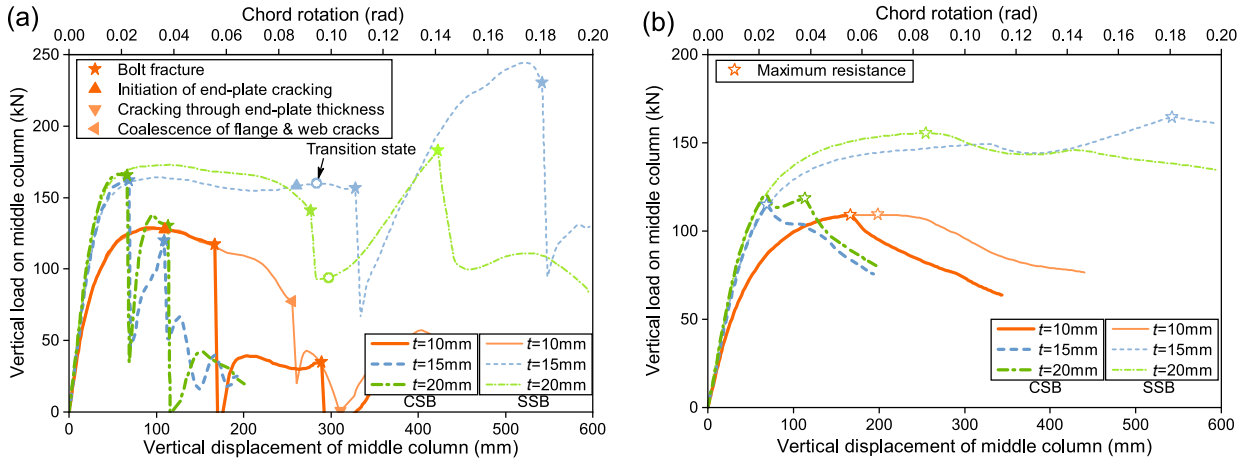

Fig. 15. Effect of end-plate thickness on load–displacement response of FEP connections (Cases 7, 8 and 9): (a) static responses; (b) pseudo-static responses.

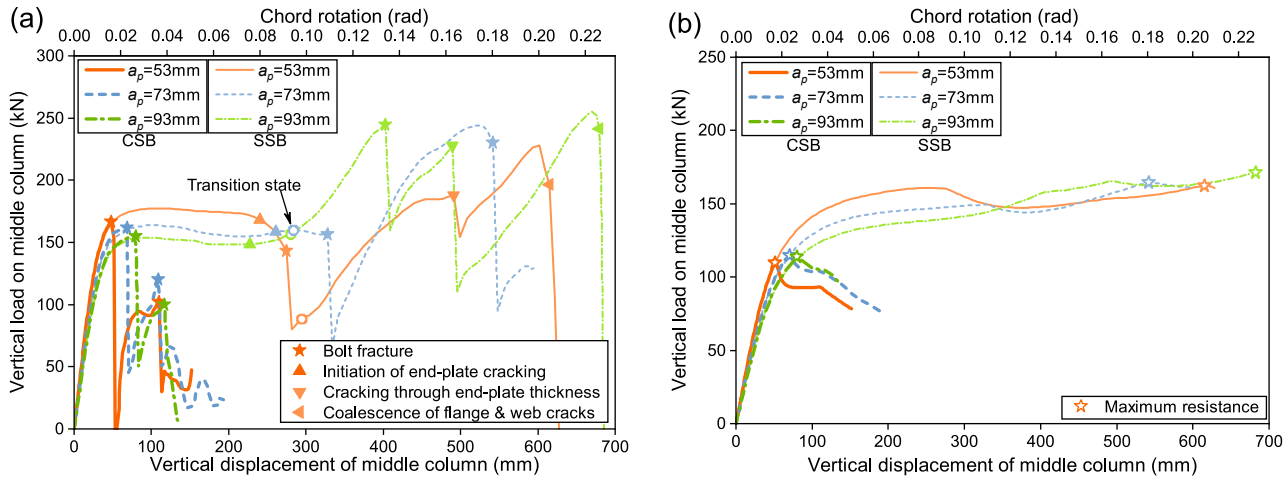

Fig. 16. Effect of bolt-row position on load–displacement response of FEP connections (Cases 5, 8 and 11): (a) static responses; (b) pseudo-static responses.

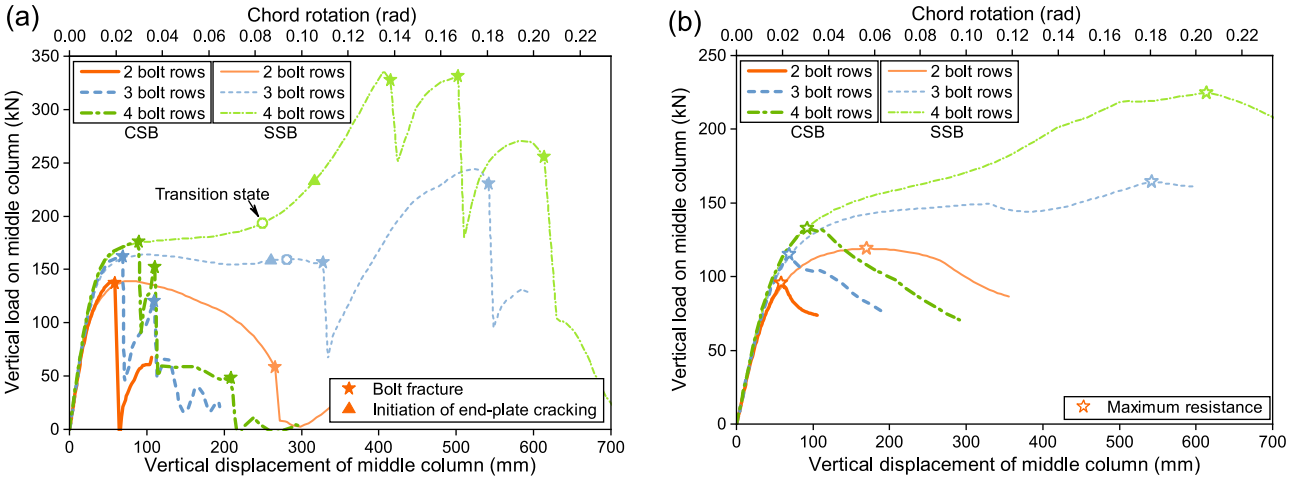

Fig. 17. Effect of number of bolt-rows on load–displacement response of FEP connections (Cases 2, 8 and 14): (a) static responses; (b) pseudo-static responses.

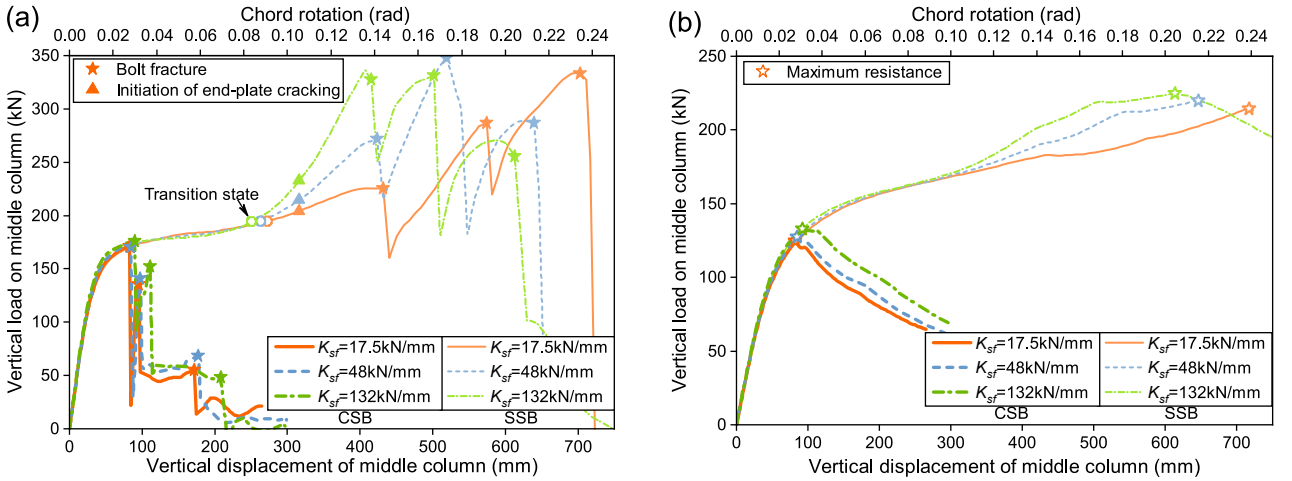

Fig. 18. Effect of lateral restraining stiffness on load–displacement response of FEP connections (Cases 14, 16 and 17): (a) static responses; (b) pseudo-static responses.

pseudo-static response (Fig. 18(b)), the maximum dynamic loads of the connections are only slightly affected by the lateral restraining stiffness. The ratio $k_{P,SSB}$ maintains basically unchanged in the three cases (see Table 2), indicating that the effectiveness of using SSB is not affected by varying the lateral restraining stiffness.

Fig. 19(a) illustrates the effect of beam span-to-depth ratio (L_b/D_b) on

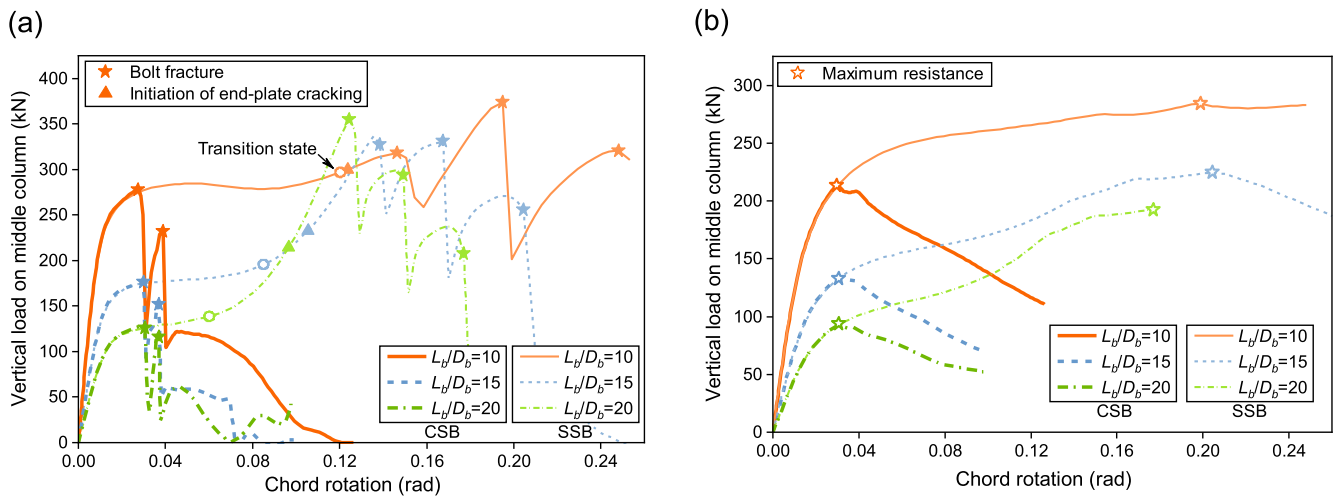

Fig. 19. Effect of beam span-to-depth ratio on load–displacement response of FEP connections (Cases 14, 18 and 19): (a) static responses; (b) pseudo-static responses.

the static load–displacement response, where one can clearly identify that in the flexure-dominant stage, the static load increases significantly with the decrease in L_b/D_b. This is however not due to the enhancement in the flexural strength, but because of the reduced lever arm (the distance between the connection and the point of contraflexure shown in Fig. 2). With the use of SSB, the transition state is significantly postponed, and the extent of catenary action is reduced with the decrease in L_b/D_b. From the pseudo-static responses (Fig. 19(b) and Table 2), it can be seen that although the maximum dynamic load increases with the decrease of L_b/D_b, the ratio $k_{P,SSB}$ decreases significantly (from 2.04 to 1.33) with the reduce of L_b/D_b from 20 to 10.

5. Parametric study of web angle (WA) connections

5.1. Overview of parameters

The performances of WA connections with and without stainless steel components are evaluated based on the configuration shown in Fig. 6 (b). To achieve the full ductility of the stainless steel components, the premature failures of the shear bolts (the ones connected to the beam web) and the beam webs in bearing/block shear were suppressed through providing more shear bolts than required, and stiffening the beam web with 10 mm doubling plates on both sides. Again, three configurational parameters (the thickness t of the web angle, the number of bolt-rows and the geometric parameter a_p) and two parameters of structural layout (the lateral restraining stiffness K_{sf} and the beam span-to-depth ratio L_b/D_b, as defined in Section 4.1) were considered. The geometric parameter a_p for WA connections is the horizontal distance between the centres of the tension bolts to the surface of the web stiffening plate (see Fig. 6(b)). Table 3 summarises the combinations of design parameters for the WA connections. A total of four combinations (scenarios) of angles and bolts were considered: (1) carbon steel angles (CSA) + carbon steel bolts (CSB), which is the benchmark condition; (2) stainless steel angles (SSA) + CSB; (3) CSA + stainless steel bolts (SSB); and (4) SSA + SSB. However, full comparisons of the four combinations were only made for Cases 6 and 8 (Section 5.3). For all the other cases, only two combinations ((1) and (4)) were considered.

5.2. Connection behaviour and failure modes

Since the flexural capacity of a normally pinned WA connection is negligible throughout the loading, the vertical load applied on the removed (middle) column is carried mostly by the catenary action, which begins to develop at a relatively small chord rotation when the clearances between the shear bolts and the bolt holes are closed. The arching action does not exist for WA connections due to the initial gap

Table 3
Summary of parameters and analysed results of WA connections.

Case No.	Configuration of connection			K_{sf} (kN/mm)	L_b/D_b	$P_{d,max}$ (kN)		$k_{P,SSAB}$	Failure mode[1] (CSAB/SSAB)
	No. of bolt-rows	a_p (mm)	t (mm)			CSAB (CSA + CSB)	SSAB (SSA + SSB)		
1	2	60	8	132	15	38.1	71.7	1.88	FB/FB
2	2	60	12	132	15	33.4	69.6	2.08	FB/FB
3	3	50	8	132	15	50.5	112.5	2.23	FBA/FB
4	3	50	10	132	15	45.4	103.0	2.27	FB/FB
5	3	50	12	132	15	44.0	111.6	2.54	FB/FB
6	3	60	8	132	15	55.8	106.9	1.92	FBA/FB
7	3	60	10	132	15	48.1	97.1	2.02	FB/FB
8	3	60	12	132	15	48.7	100.8	2.07	FB/FB
9	3	70	8	132	15	52.9	106.2	2.01	FA/FB
10	3	70	10	132	15	50.7	93.7	1.85	FB/FB
11	3	70	12	132	15	48.5	94.2	1.94	FB/FB
12	4	60	8	132	15	62.1	130.4	2.10	FBA/FB
13	4	60	12	132	15	57.9	128.1	2.21	FB/FB
14	3	60	10	17.5	15	49.0	99.0	2.02	FB/FB
15	3	60	10	48	15	47.4	97.0	2.05	FB/FB
16	3	60	10	132	10	59.0	116.5	1.97	FB/FB
17	3	60	10	132	20	42.9	87.3	2.03	FB/FB

[1] : Abbreviations of the failure modes: “FB”-Fracture of bolts; “FA”-Fracture of web angle; “FBA”-Fracture of bolts with cracking in the web angle.

between the beam end and the column surface.

Again, three failure modes were obtained for WA connections, i.e., angle fracture (Mode FA), bolt fracture (Mode FB) and a combined mode (Mode FBA). For mode FA (Fig. 20), the initial cracking at the root of an angle typically developed much faster than that in an end-plate, which is due to the more uniform stress distribution across the angle section. Consequently, the vertical load/axial force dropped rapidly after the 1st cracking, making it impossible for any force re-distribution or re-ascending of load.

Fig. 21 illustrates a typical failure process of Mode FB. Similar to Mode FB of FEP connections, the failure was caused by successive fractures of the bolts from the bottom to the top, each corresponding with a sudden drop in the vertical load/axial force. Due to the strong catenary action in WA connections, the sudden load drop was always followed by an immediate re-ascending branch due to the force redistribution among the remaining bolt-rows. The maximum dynamic load was typically achieved right before the fracture of the last bolt-row. Furthermore, it was noted that the SSB in the WA connections exhibited a distinct fracture mode with combined tension and shear, which is due to the membrane action of the web angles when subjecting to large deformations (Fig. 22). This particular fracture mode was not observed for CSB due to their relatively low ductility, hence the membrane action cannot be developed.

Fig. 23 shows a typical failure process of Mode FBA. Different from Mode FBE of FEP connections, the cracking of angle typically occurred at the end of loading, after the fractures of all except the last (top) bolt-rows. The identified failure modes of all the WA connections are summarised in Table 3. Due to the relatively high deformation capacity of web angles, Mode FB was observed in 30 out of the total 34 cases (including all the 17 cases with SSA). Web angle cracking only occurred in the 8 mm thick carbon steel angles.

5.3. Different combinations of components

Fig. 24 shows the static and pseudo static load–displacement responses with different combinations of angle and bolt materials, where the values of the maximum dynamic loads with the four combinations of angles and bolts are also given (Fig. 24(b) and (d)). For Case 6 where 8 mm web angles are employed (Fig. 24(a) and (b)), the use of stainless steel angles alone (SSA + CSB) did not produce significant enhancement in either the static or pseudo-static performance comparing with the benchmark scenario (CSA + CSB). This is due to the premature failures of CSB in both scenarios. The use of stainless steel bolts alone (CSA + SSB) led to slight increases in the maximum static and dynamic loads (in comparison with the benchmark scenario). However, in this scenario the load resistance was limited by the fracture of CSA. As expected, the highest load resistance was obtained through the combined use of SSA and SSB: the maximum static and dynamic loads were nearly doubled compared with the benchmark scenario.

For Case 8 where 12 mm web angles were used (Fig. 24(c) and (d)), the connections failed by Mode FB in all the scenarios. Therefore, the performance is primarily related to the ductility of the tension bolts. As can be seen in Fig. 24(c), with the use of SSB, the maximum static load and the rotation capacity (the chord rotation at final failure) are both significantly enhanced. The maximum dynamic load is increased by more than one time comparing with the benchmark scenario with CSA and CSB (Fig. 24(d)). It can be also noted that with the use of SSB, the adoption of either CSA or SSA has barely any effect on the overall response.

From the above comparisons, it can be seen that the use of both SSA and SSB seems to be necessary to guarantee the expected enhancement in the collapse resistance (especially in the cases with thin web angles). In the remaining of this section, only one scenario with stainless steel angles and bolts (SSA + SSB, or SSAB) is considered along with the benchmark scenario (CSA + CSB, or CSAB) for each of the cases.

5.4. Effect of connection configuration

The effect of web angle thickness t is demonstrated in Fig. 25. It can be seen that the maximum static load and the rotation capacity are both enhanced, whilst the stiffness of the ascending branch is decreased, with the decrease in angle thickness (Fig. 25(a)). This is due to the relatively high flexibility of thinner web angles. Cracking of web angle only occurred in CSA at relatively large rotations (well after 2nd bolt fracture), hence had limited influence on the overall performance. From Fig. 25(b) and Table 3, it can be seen that the maximum dynamic load $P_{d,\max}$, and the ratio of the maximum dynamic loads with stainless steel and carbon steel components ($k_{P,SSAB}$) are barely affected by the angle thickness.

As shown in Fig. 26(a), with the decrease in distance a_p, the stiffness of the ascending branch is enhanced, whilst the maximum static load decreases slightly due to earlier fracture of the 1st bolt-row. Moreover, a carbon steel web angle with smaller a_p appears to be less prone to angle cracking. As shown in Fig. 26(b) and Table 3, there is no clear relationship between $P_{d,\max}$ (as well as $k_{P,SSAB}$) and the position of bolts.

It can be seen from Fig. 27(a) that by increasing the number of bolt-rows, all the characteristics related to the collapse-resisting performance, i.e., the stiffness of the ascending branch, the maximum static load, as well as the rotation capacity, are enhanced. Consequently, the maximum dynamic load and the ratio $k_{P,SSAB}$ both increase substantially

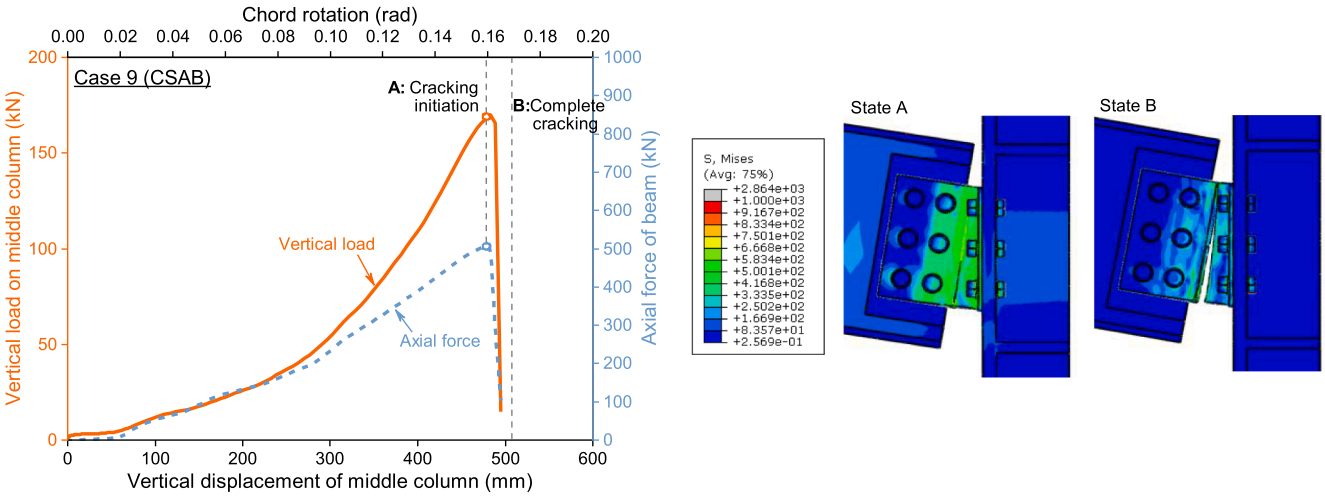

Fig. 20. Failure of WA connections with angle fracture (Mode FA).

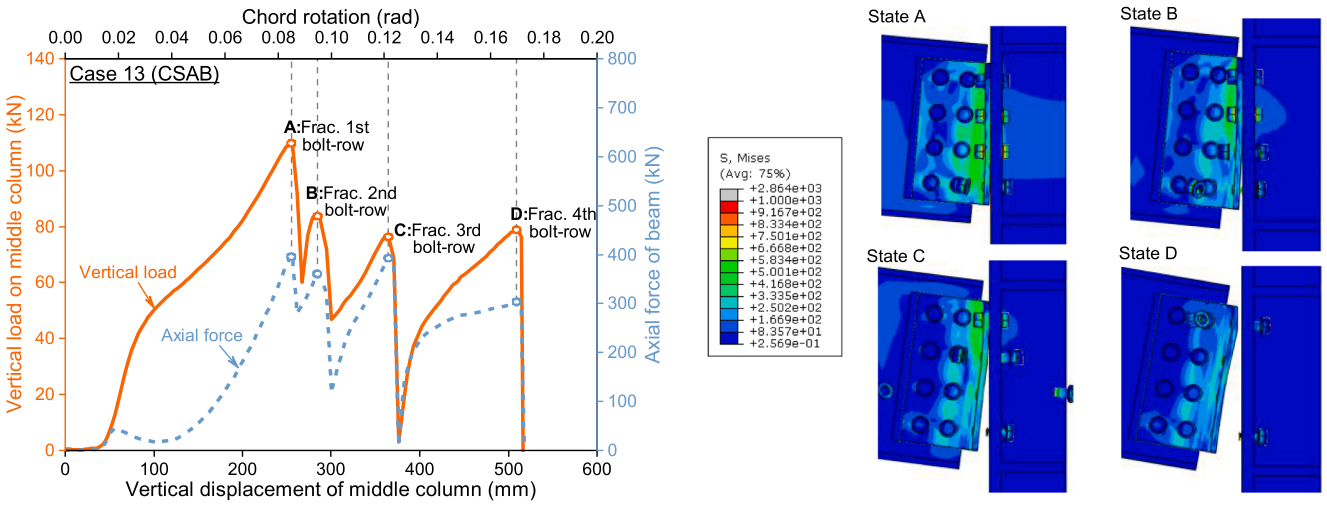

Fig. 21. Failure of WA connections with bolt fractures (Mode FB).

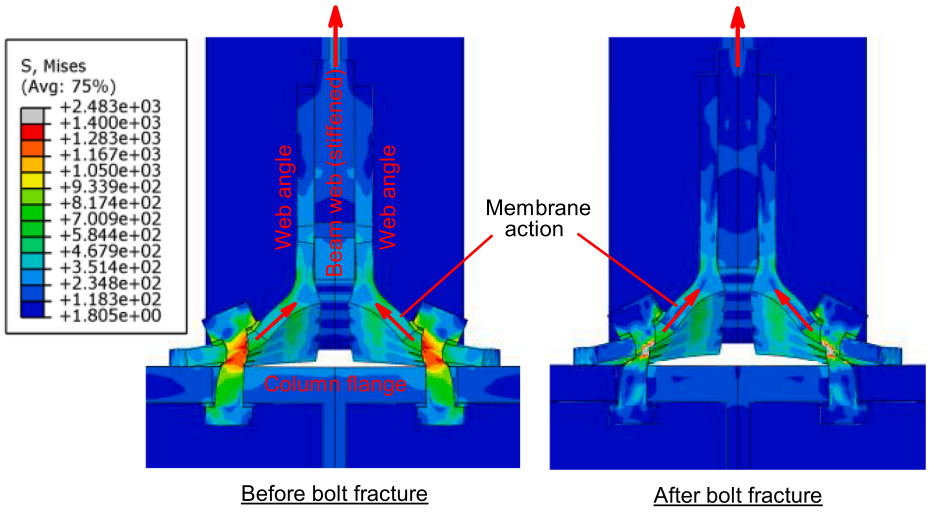

Fig. 22. Combined tension & shear fracture of stainless steel bolts in WA connections.

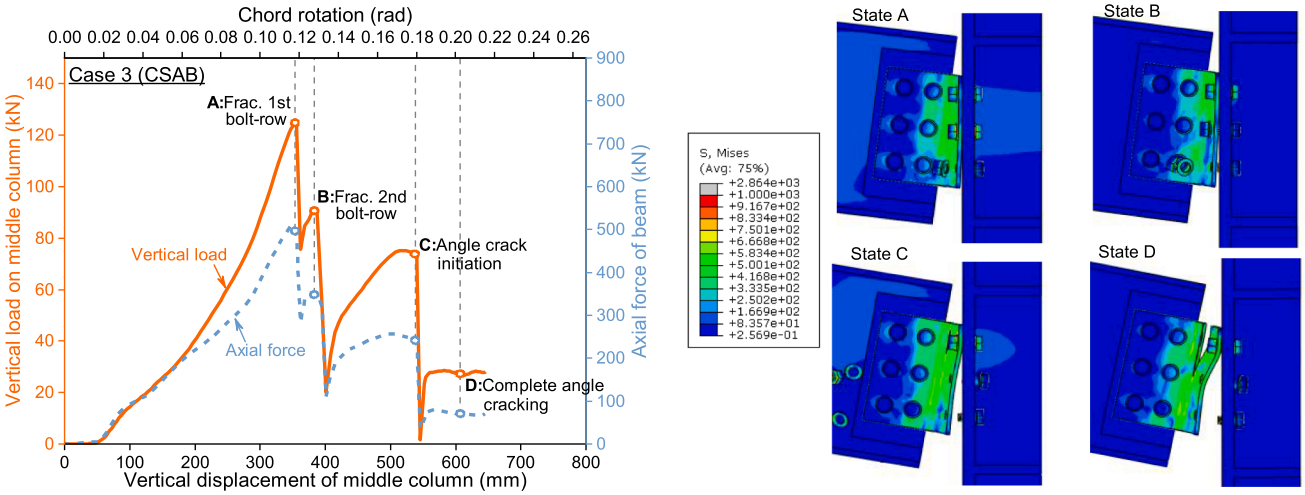

Fig. 23. Failure of WA connections with combined fractures of angle and bolts (Mode FBA).

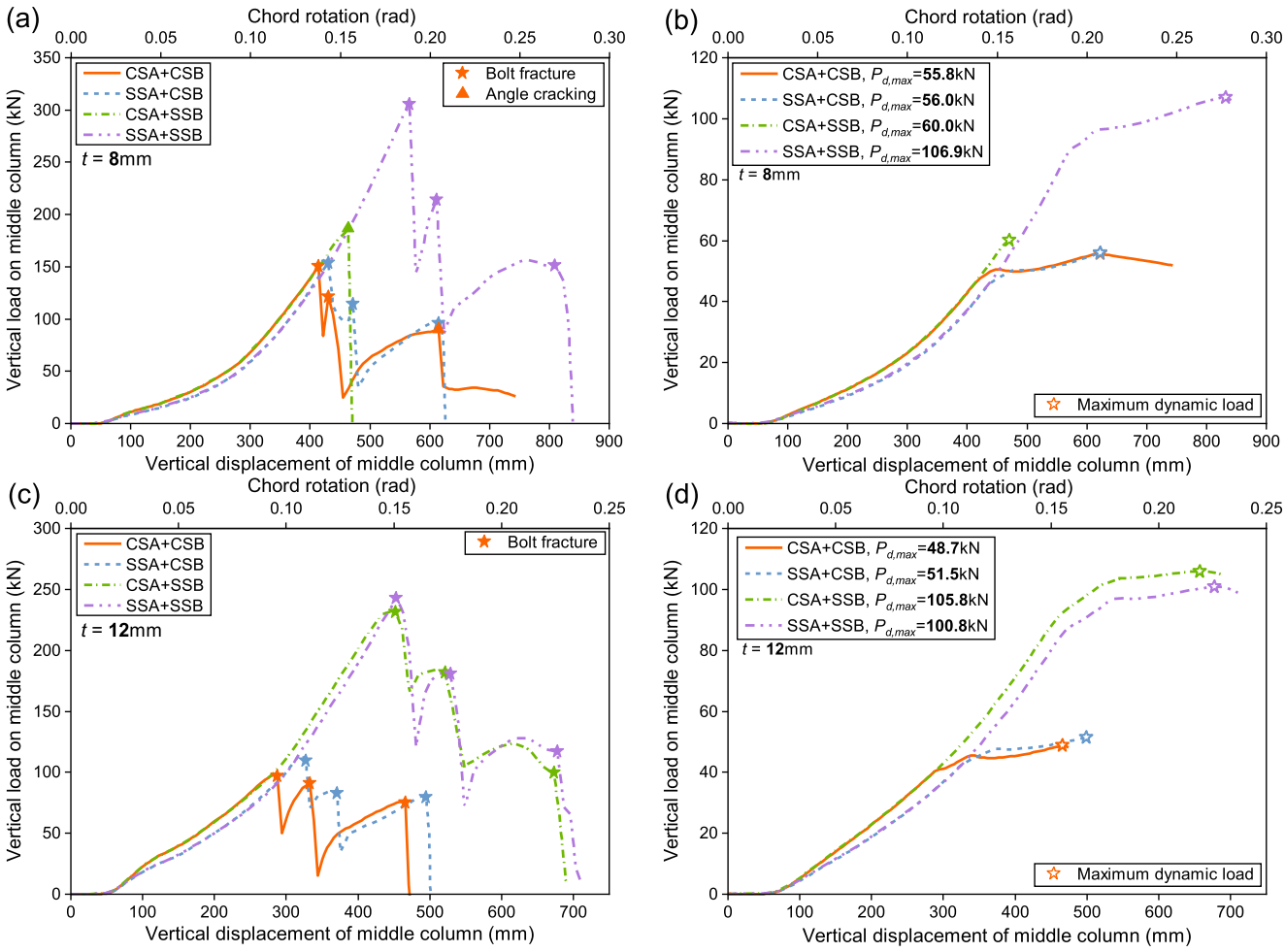

Fig. 24. Performances of WA connections with different combinations of stainless steel components: (a) static responses with 8 mm web angle (Case 6); (b) pseudo-static responses with 8 mm web angle (Case 6); (c) static responses with 12 mm web angle (Case 8); (d) pseudo-static responses with 12 mm web angle (Case 8).

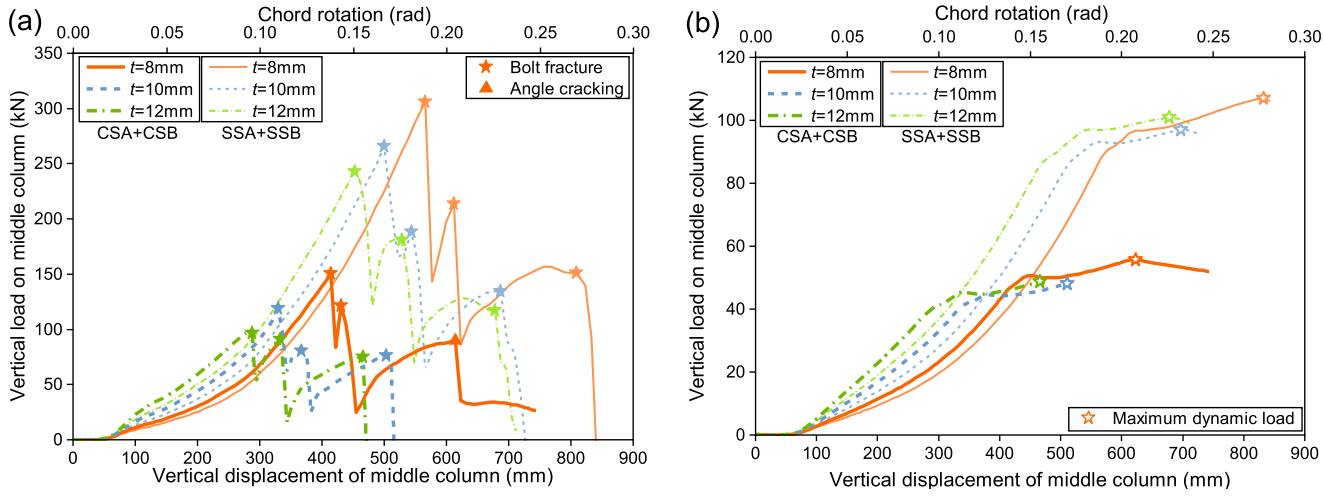

Fig. 25. Effect of thickness of web angle on load–displacement response of WA connections (Cases 6,7 and 8): (a) static responses; (b) pseudo-static responses.

with the number of bolt-rows (Fig. 27(b) and Table 3).

5.5. Effect of structural layout

As shown in Fig. 28(a), an increase in the lateral restraining stiffness (K_{sf}) enhances the stiffness of the ascending branch, whilst the maximum static load and the rotation capacity are only slightly affected. As can be seen in Fig. 28(b) and Table 3, the maximum dynamic loads and the ratio $k_{P,SSAB}$ are barely influenced by the magnitude of K_{sf}.

With a reduction in the beam span-to-depth ratio (L_b/D_b), the stiffness of the ascending branch is decreased, whilst the maximum static load and the rotation capacity are both increased (Fig. 29(a)). Although

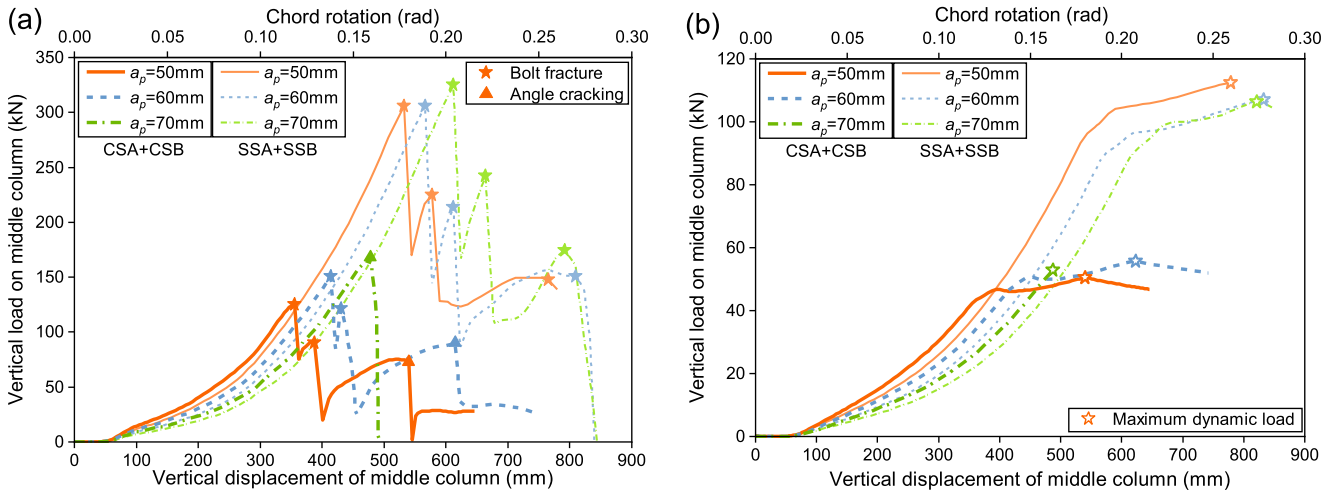

Fig. 26. Effect of bolt position on load–displacement response of WA connections (Cases 3, 6 and 9): (a) static responses; (b) pseudo-static responses.

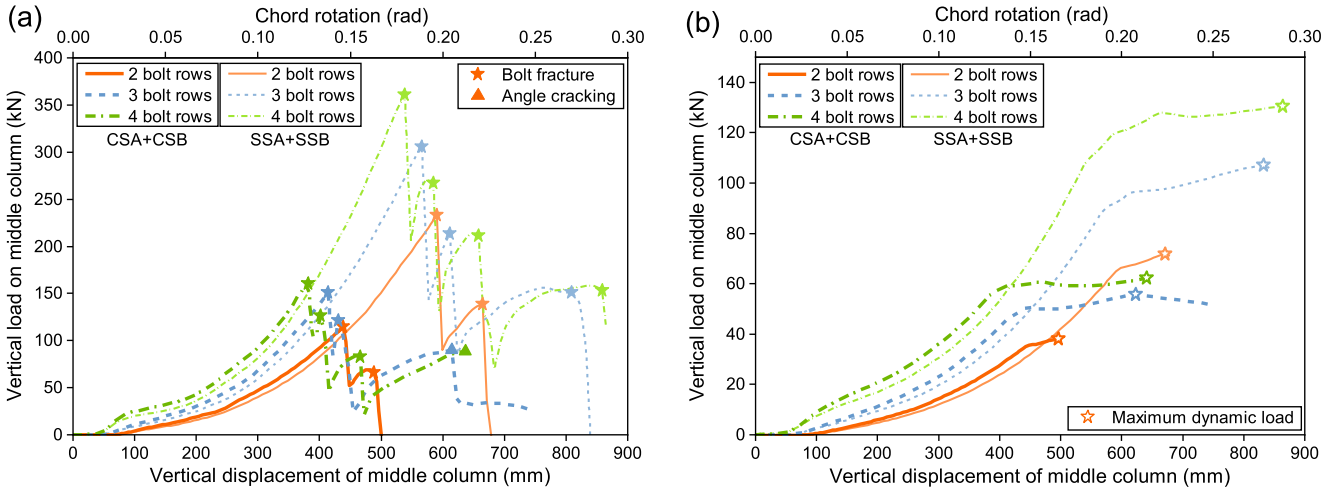

Fig. 27. Effect of number of bolt-rows on load–displacement response of WA connections (Cases 1, 6 and 12): (a) static responses; (b) pseudo-static responses.

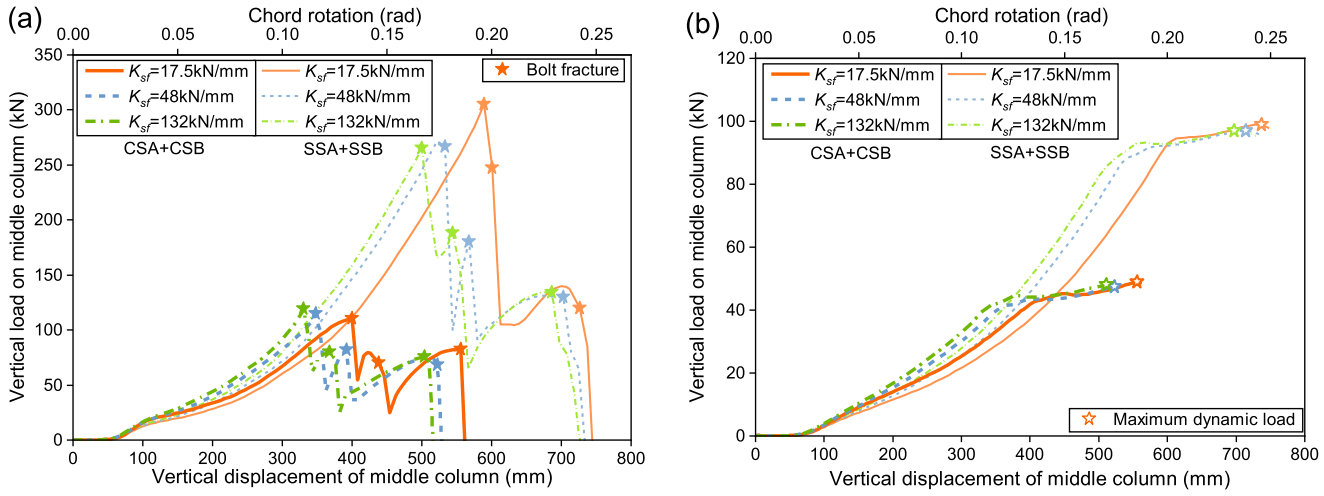

Fig. 28. Effect of lateral restraining stiffness on load–displacement response of WA connections (Cases 7, 14 and 15): (a) static responses; (b) pseudo-static responses.

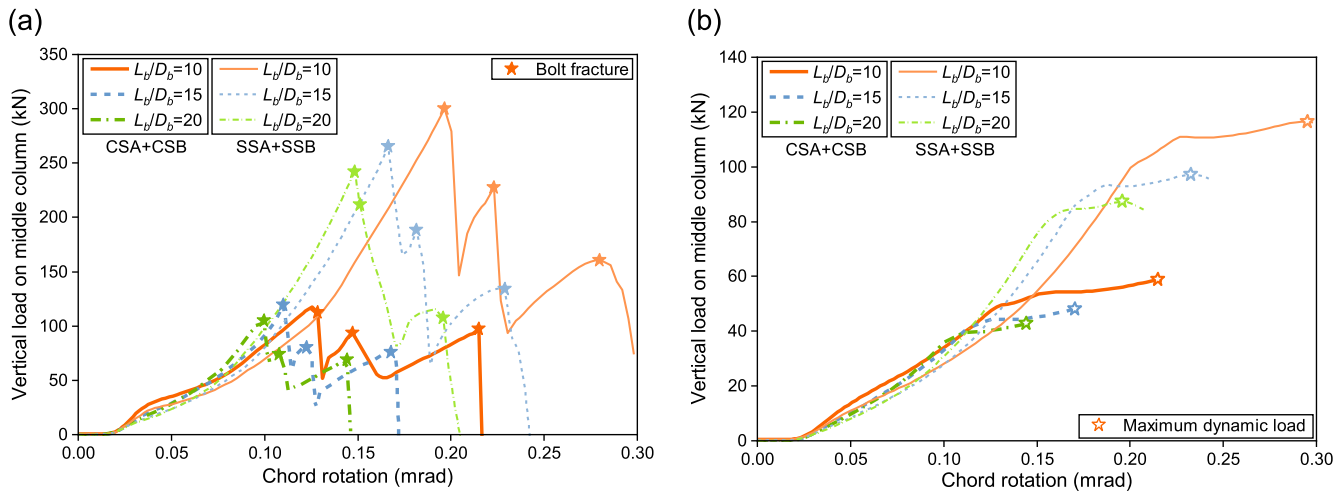

Fig. 29. Effect of beam span-to-depth ratio on load–displacement response of WA connections (Cases 7, 16 and 17): (a) static responses; (b) pseudo-static responses.

higher maximum dynamic loads were obtained with smaller span-to-depth ratios (Fig. 29(b)), it can be seen from Table 3 that the ratio $k_{P,SSAB}$ maintains basically constant with different L_b/D_b.

6. Evaluation of results and recommendations on connection configuration

From the parametric study, the two performance indexes, i.e., the maximum dynamic load with the use of stainless steel components ($P_{d,\max,SSB}$ or $P_{d,\max,SSAB}$), as well as the ratio of maximum dynamic loads with and without stainless steel components ($k_{P,SSB}$ or $k_{P,SSAB}$) were extracted (summarised in Tables 2 and 3) and are visualised in Fig. 30 for FEP and WA connections with different configurations. Overall, the FEP connections with SSB exhibit higher maximum dynamic loads (red columns in Fig. 30) than the WA connections with SSA and SSB, which is mainly attributed to the higher early-stage capacities (due to the flexural and arching actions) of the former. Nevertheless, the use of stainless steel components in WA connections is much more effective than that in FEP connections. This can be seen from the higher dynamic load ratios of WA connections (mean and maximum values of $k_{P,SSAB}$ are 2.09 and 2.54, respectively) than those of FEP connections (mean and maximum values of $k_{P,SSB}$ are 1.30 and 1.69). This is due to the greater contribution of the catenary action (hence the collapse resistance relies more on the component ductility) in WA connections.

For FEP connections (Fig, 30(a)), it is clear that the use of SSB with thin (in this study 10 mm) end-plates should be avoided: as it could significantly detriment both $P_{d,\max,SSB}$ and $k_{P,SSB}$, due to premature end-plate fractures before achieving the full ductility of SSB. The use of 15 mm end-plate seems to be an optimum choice among all the cases as it is sufficient to control the development of end-plate cracking, whilst still enables some bending deformations of the end-plate before bolt fractures. The change of bolt position (by varying a_p) does not have significant effect on both $P_{d,\max,SSB}$ and $k_{P,SSB}$. For WA connections, the effect of configuration seems to be insignificant, though slightly higher $P_{d,\max,SSAB}$ can be achieved with the tension bolts placed closer to the beam web (smaller a_p). For both FEP and WA connections, the increase in the number of bolt-rows could significantly enhance the absolute maximum dynamic load and the effectiveness of using stainless steel components.

7. Conclusions

This paper proposed the use of stainless steel components for enhancing the progressive collapse resistance of flush end-plate (FEP) and web angle (WA) beam-to-column connections. The core idea is to replace the critical connection components (bolts and web angles), that are subjected to large deformation demands, with highly ductile (austenitic) stainless steel counterparts, hence achieving enhancements in both connection ductility and ultimate load capacity. To quantitatively assess the viability and effectiveness of this concept, finite element (FE) push-down analyses were carried out simulating a middle column removal scenario. Specifically, the constitutive and fracture models were calibrated against previous material tests of carbon/stainless steel

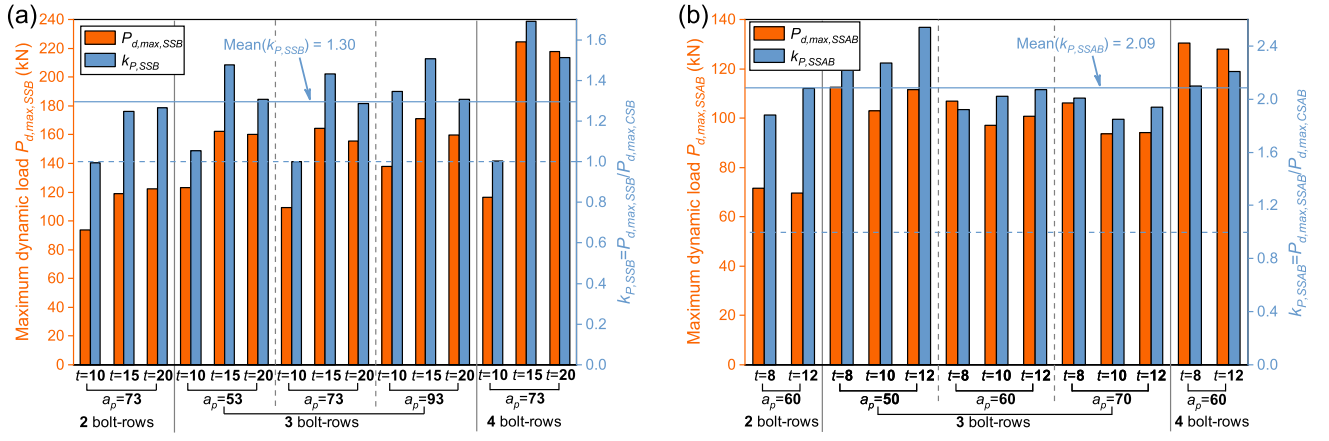

Fig. 30. Summary and evaluation of collapse-resisting performances: (a) FEP connections with stainless steel bolts; (b) WA connections with stainless steel bolts and angles.

components to accurately predict their failure modes. The FE models were validated against available sub-structure tests of FEP and WA connections. Thereafter, an extensive parametric study was performed to investigate the behaviours of connections with and without stainless steel components, as well as the effects of various configurations and structural layouts. Two performance indexes, i.e. the absolute maximum dynamic load, and the ratio of maximum dynamic loads with and without stainless steel components, were introduced to evaluate the collapse resistance of the connections. The following conclusions are drawn from this research:

- The use of stainless steel bolts (SSB) instead of carbon steel bolts (CSB) in FEP connections generally led to remarkable increases in the deformation capacity. Consequently, the development of catenary action could be guaranteed, and the maximum dynamic load was increased by around 30 % on average.
- For WA connections, the use of stainless steel angles (SSA) alone did not produce significant improvement in performance due to the limited ductility of CSB. On the other hand, the use of SSB alone led to significant enhancements in deformation and load capacities, provided the web angles have sufficient ductility against premature cracking. The combined use of SSA and SSB produced the most satisfied performance: the maximum dynamic load was enhanced by 109 % on average compared with the benchmark conditions with all carbon steel components.
- To fully exploit the ductility of SSB in FEP connections, the use of relatively thick end-plates are recommended in order to avoid premature failures due to end-plate fractures. The position of bolt-rows seemed to have limited influence on the collapse resistance of FEP connections
- The thickness of web angle does not have notable effect on the collapse resistance if both SSB and SSA are used in WA connections. With tension bolts placed closer to the beam web, the collapse resistance of WA connections was slightly enhanced.
- For both FEP and WA connections, increasing the number of tension bolt-rows could provide additional redundancy and enable force redistribution after partial failure. Hence, the deformation and load capacities can be both increased, leading to a remarkable enhancement in the collapse resistance.
- The lateral restraining stiffness of surrounding spans had limited influence on the resistance of connections in the collapsing spans (directly affected by the removed column). A decrease in the beam span-to-depth ratio could enhance the vertical load resistance due to the reduced lever arm.
- It is proved in this study that the use of ductile stainless steel components could effectively improve the ductility of beam-to-column connections, hence guarantee the development of catenary action and enhance the progressive collapse resistance. This enhancement was confirmed for a wide range of cases with few limitations on the connection configuration. Considering the very competitive cost-efficiency, as well as the minor modifications to exiting design and construction practices, the proposed concept has great potential to benefit new designs and retrofitting works, provided the special design requirements (e.g. the galvanic corrosion consideration and the differences in bolt preload and fiction factor) of stainless steel components are well recognised. The concept could be extended to many other scenarios (other than the FEP and WA connections), where the ductility of a few critical components controls the robustness of the entire system.

CRediT authorship contribution statement

Yuchen Song: Conceptualization, Methodology, Software, Formal analysis, Investigation, Visualization, Writing – original draft. **Michael C.H. Yam:** Conceptualization, Resources, Supervision, Funding acquisition, Investigation, Writing – review & editing. **Junjie Wang:** Conceptualization, Methodology, Investigation, Writing – original draft, Writing – review & editing.

Declaration of Competing Interest

The authors declare that they have no known competing financial interests or personal relationships that could have appeared to influence the work reported in this paper.

Data availability

Data will be made available on request.

Acknowledgements

The work presented in this paper is fully supported by a grant from the Chinese National Engineering Research Centre (CNERC) for Steel Construction (Hong Kong Branch) at The Hong Kong Polytechnic University (Project No.: BBVW).

References

[1] Starossek U. Progressive collapse of structures. London: Thomas Telford; 2009.
[2] Li H. Modeling, behavior and design of collapse-resistant steel frame buildings. University of Michigan; 2013.
[3] Qiao H, Yang Y, Zhang J. Progressive Collapse Analysis of Multistory Moment Frames with Varying Mechanisms. J Perform Construct Facil 2018;32(4):04018043.
[4] Wang J, Ke K, Wang W. Structural robustness evaluation of steel frame buildings with different composite slabs using reduced-order modeling strategies. J Const Steel Res 2022;196:107371.
[5] Johnson ES, Meissner JE, Fahnestock LA. Experimental Behavior of a Half-Scale Steel Concrete Composite Floor System Subjected To Column Removal Scenarios. J Struct Eng 2016;142(2):04015133.
[6] Hadjioannou M, Donahue S, Williamson EB, Engelhardt M, D.,. Large-Scale Experimental Tests of Composite Steel Floor Systems Subjected to Column Loss Scenarios. J Struct Eng 2018;144(2):04017184.
[7] Fu QN, Tan KH, Zhou XH, Yang B. Three-Dimensional Composite Floor Systems under Column-Removal Scenarios. J Struct Eng 2018;144(10):04018196.
[8] Zandonini R, Baldassino N, Freddi F, Roverso G. Steel-concrete frames under the column loss scenario: An experimental study. J Const Steel Res 2019;162:105527.
[9] Wang J, Wang W, Bao Y, Lehman D. Full-scale test of a steel moment-resisting frame with composite floor under a penultimate edge column removal scenario. J Const Steel Res 2019;162:105717.
[10] Wang J, Wang W, Bao Y. Full-Scale Test of a Steel-Concrete Composite Floor System with Moment-Resisting Connections under a Middle-Edge Column Removal Scenario. J Struct Eng 2020;146(5):04020067.
[11] Zhang J-Z, Li G-Q, Jiang J. Collapse of steel-concrete composite frame under edge-column loss—Experiment and its analysis. Eng Struct 2020;209:109951.
[12] Ren L-M, Yang B, Chen K, Sun Y-J, Kong D-Y. Progressive Collapse of 3D Composite Floor Systems with Rigid Connections under External Column Removal Scenarios. J Struct Eng 2020;146(11):04020244.
[13] Guo L, Gao S, Fu F, Wang Y. Experimental study and numerical analysis of progressive collapse resistance of composite frames. J Const Steel Res 2013;89:236–51.
[14] Dinu F, Marginean I, Dubina D. Experimental testing and numerical modelling of steel moment-frame connections under column loss. Eng Struct 2017;151:861–78.
[15] Yang B, Tan KH. Experimental tests of different types of bolted steel beam–column joints under a central-column-removal scenario. Eng Struct 2013;54:112–30.
[16] Wang W, Fang C, Qin X, Chen Y, Li L. Performance of practical beam-to-SHS column connections against progressive collapse. Eng Struct 2016;106:332–47.
[17] Zhu C, Rasmussen KJR, Yan S, Zhang H. Experimental full-range behavior assessment of bolted moment end-plate connections. J Struct Eng 2019;145(8):04019079.
[18] Yan S, Jiang L, Rasmussen KJR. Full-range behaviour of double web angle connections. J Constr Steel Res 2020;166:105907.
[19] Kukla D, Kozlowski A. Parametric study of steel flush and extended end-plate joints under column loss scenario. Eng Struct 2021;237:112204.
[20] Yang B, Tan KH. Robustness of Bolted-Angle Connections against Progressive Collapse: Experimental Tests of Beam-Column Joints and Development of Component-Based Models. J Struct Eng 2013;139(9):1498–514.
[21] Sadek F, Main JA, Lew HS, Bao Y. Testing and Analysis of Steel and Concrete Beam-Column Assemblies under a Column Removal Scenario. J Struct Eng 2011;137(9):881–92.
[22] Li L, Wang W, Chen Y, Lu Y. Effect of beam web bolt arrangement on catenary behaviour of moment connections. J Const Steel Res 2015;104:22–36.
[23] Xie Z, Chen Y. Numerical study of the robustness of steel moment connections under catenary effect. Eng Struct 2022;252:113658.

[24] Qin X, Wang W, Chen Y, Bao Y. A special reinforcing technique to improve resistance of beam-to-tubular column connections for progressive collapse prevention. Eng Struct 2016;117:26–39.
[25] Lu X, Zhang L, Lin K, Li Y. Improvement to composite frame systems for seismic and progressive collapse resistance. Eng Struct 2019;186:227–42.
[26] Wang J, Wang W. Macromodeling Approach and Robustness Enhancement Strategies for Steel Frame Buildings with Composite Slabs against Column Loss. J Struct Eng 2022;148(1):04021238.
[27] Alrubaidi M, Abbas H, Elsanadedy H, Almusallam T, Iqbal R, Al-Salloum Y. Experimental and FE study on strengthened steel beam-column joints for progressive collapse robustness under column-loss event. Eng Struct 2022;258:114103.
[28] Wei J-P, Tian L-M, Hao J-P, Li W, Zhang C-B, Li T-J. Novel principle for improving performance of steel frame structures in column-loss scenario. J Const Steel Res 2019;163:105768.
[29] Qiao H, Xia J, Chen Y, Chen C, Zheng J. A novel principle for improving collapse resistance of steel frame structures. J Const Steel Res 2022;196:107408.
[30] Baddoo NR. Stainless steel in construction: A review of research, applications, challenges and opportunities. J Constr Steel Res 2008;64(11):1199–206.
[31] Gardner L. The use of stainless steel in structures. Prog Struct Engng Mater 2005;7(2):45–55.
[32] Han L-H, Xu C-Y, Tao Z. Performance of concrete filled stainless steel tubular (CFSST) columns and joints: Summary of recent research. J Constr Steel Res 2019;152:117–31.
[33] Di Sarno L, Elnashai AS, Nethercot DA. Seismic performance assessment of stainless steel frames. J Constr Steel Res 2003;59(10):1289–319.
[34] Di Sarno L, Elnashai AS, Nethercot DA. Seismic response of stainless steel braced frames. J Constr Steel Res 2008;64(7):914–25.
[35] Di Sarno L, Elnashai AS, Nethercot DA. Seismic retrofitting of framed structures with stainless steel. J Constr Steel Res 2006;62(1):93–104.
[36] Culache G, Byfield MP, Ferguson NS, Tyas A. Robustness of Beam-to-Column End-Plate Moment Connections with Stainless Steel Bolts Subjected to High Rates of Loading. J Struct Eng 2017;143(6):04017015.
[37] Satheeskumar N, Davison JB. Robustness of steel joints with stainless steel bolts in fire. Int J Adv Struct Eng 2014;6(4):161–8.
[38] Song Y, Wang J, Uy B, Li D. Experimental behaviour and fracture prediction of austenitic stainless steel bolts under combined tension and shear. J Constr Steel Res 2020;166:105916.
[39] Y. Song, J. Wang, B. Uy, D. Li, Stainless steel bolts subjected to combined tension and shear: behaviour and design, J. Constr. Steel Res. (2020).
[40] Elflah M, Theofanous M, Dirar S, Yuan H. Behaviour of stainless steel beam-to-column joints-Part 1: Experimental investigation. J Constr Steel Res 2019;152:183–93.
[41] Elflah M, Theofanous M, Dirar S, Yuan H. Structural behaviour of stainless steel beam-to-tubular column joints. Eng Struct 2019;184:158–75.
[42] Hasan MJ, Al-Deen S, Ashraf M. Behaviour of top-seat double web angle connection produced from austenitic stainless steel. J Constr Steel Res 2019;155:460–79.
[43] Gao JD, Yuan HX, Du XX, Hu XB, Theofanous M. Structural behaviour of stainless steel double extended end-plate beam-to-column joints under monotonic loading. Thin-Walled Struct 2020;151:106743.
[44] Song Y, Uy B, Li D, Wang J. Ultimate behaviour and rotation capacity of stainless steel end-plate connections. Steel Compos Struct 2022;42(4):569–90.
[45] Bu Y, Wang Y, Zhao Y. Study of stainless steel bolted extended end-plate joints under seismic loading. Thin-Walled Struct 2019;144:106255.
[46] Song Y, Wang J, Uy B, Li D. Behaviour and design of stainless steel-concrete composite beam-to-column joints. J Constr Steel Res 2021;184:106800.
[47] Wang J, Uy B, Li D, Song Y. Progressive collapse analysis of stainless steel composite frames with beam-to-column endplate connections. Steel Compos Struct 2020;36(4):427–46.
[48] Ghorbanzadeh B, Bregoli G, Vasdravellis G, Karavasilis TL. Pilot experimental and numerical studies on a novel retrofit scheme for steel joints against progressive collapse. Eng Struct 2019;200:109667.
[49] Bregoli G, Vasdravellis G, Karavasilis TL, Cotsovos DM. Static and dynamic tests on steel joints equipped with novel structural details for progressive collapse mitigation. Eng Struct 2021;232:111829.
[50] A designers' handbook series: Welding of stainless steels and other joining methods, American Iron and Steel Institute, Washington, 1988.
[51] EN1993-1-4, Eurocode 3: Design of Steel Structures, Part 1-4: General rules-Supplementary rules for stainless steels, Comité Européen de Normalisation, Brussels, Belgium, 2015.
[52] Afzali N, Stranghöner N, Pilhagen J, Manninen T, Schedin E. Viscoplastic deformation behaviour of preloaded stainless steel connections. J Constr Steel Res 2019;152:225–34.
[53] Stranghöner N, Afzali N, de Vries P, Schedin E, Pilhagen J. Slip factors for slip-resistant connections made of stainless steel. J Constr Steel Res 2019;152:235–45.
[54] Zheng B, Wang J, Gu Y, Shu G, Xie J, Jiang Q. Experimental study on stainless steel high-strength bolted slip-resistant connections. Eng Struct 2021;231:111778.
[55] Yang B. The behaviour of steel and composite structures under a middle-column-removal scenario. Nanyang Technological University; 2013.
[56] Stranghöner N, Abraham C. Shear resistance of austenitic and duplex stainless steel bolts. J Constr Steel Res 2021;184:106807.
[57] Song Y. Behaviour and design of stainless steel and stainless steel-concrete composite beam-to-column joints with end-plate connections. The University of Sydney; 2022.
[58] Rice JR, Tracey DM. On the ductile enlargement of voids in triaxial stress fields. J Mech Phys Solids 1969;17(3):201–17.
[59] Yang F, Liu Y, Xin H, Veljkovic M. Fracture simulation of a demountable steel-concrete bolted connector in push-out tests. Eng Struct 2021;239:112305.
[60] Y.W. Lee, T. Wierzbicki, Quick Fracture Calibration for Industrial Use, No. 115, Impact and Crashworthiness Laboratory, Massachusetts Institute of Technology, 2004.
[61] Li D, Uy B, Wang J, Song Y. Behaviour and design of Grade 10.9 high-strength bolts under combined actions. J Constr Steel Res 2020.
[62] Kong D-Y, Yang Y, Yang B, Zhou X-H. Experimental Study on Progressive Collapse of 3D Steel Frames under Concentrated and Uniformly Distributed Loading Conditions. J Struct Eng 2020;146(4):04020017.
[63] Li H, Cai X, Zhang L, Zhang B, Wang W. Progressive collapse of steel moment-resisting frame subjected to loss of interior column: Experimental tests. Eng Struct 2017;150:203–20.
[64] ABAQUS, User's Manual, Version 2016, Dassault Systemes Corp., Providence, RI, USA, 2016.
[65] Yang B, Tan KH. Numerical analyses of steel beam–column joints subjected to catenary action. J Constr Steel Res 2012;70:1–11.
[66] Izzuddin BA, Vlassis AG, Elghazouli AY, Nethercot DA. Progressive collapse of multi-storey buildings due to sudden column loss — Part I: Simplified assessment framework. Eng Struct 2008;30(5):1308–18.